VII.
The Extragalactic Sources and Ultra High Energy Cosmic Rays

Astroparticle Physics a.a. 2021/22

Maurizio Spurio
Università di Bologna e INFN
maurizio.spurio@unibo.it

Content

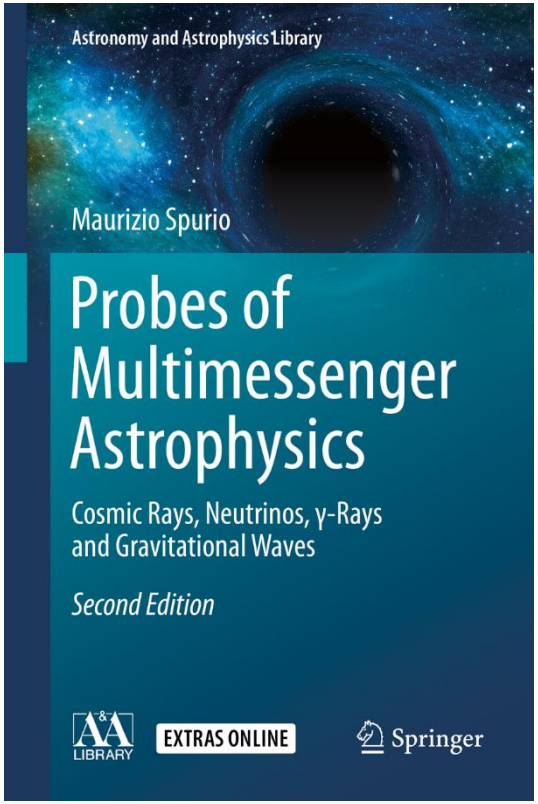

Anisotropy of UHECRs: Extragalactic Magnetic Fields

- **CR with energies above 10^{19} eV are usually referred as Ultra High Energy CRs (UHECRs)**
- Magnetic fields affect also the propagation of UHECRs, because charged particles are deflected, emitting synchrotron radiation.
- For protons, synchrotron losses are negligible, except close to sources.
- Above 10^{19} eV, the galactic magnetic field would not even trap iron nuclei very effectively. This motivated the idea of **extragalactic sources of CRs**.
- Extragalactic magnetic fields are very little known (only upper limits known)

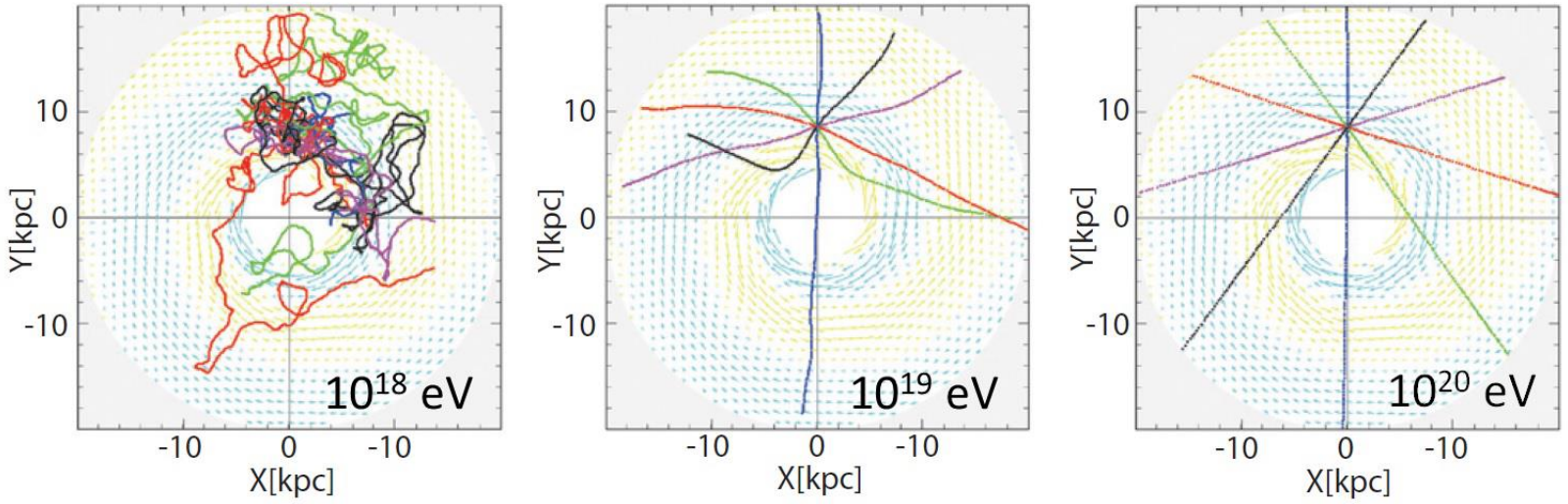

Simulated trajectory of CRs in the galactic magnetic field. Low-energy charged particles are bent by magnetic fields, but those above 10^{20} eV travel along almost straight trajectories

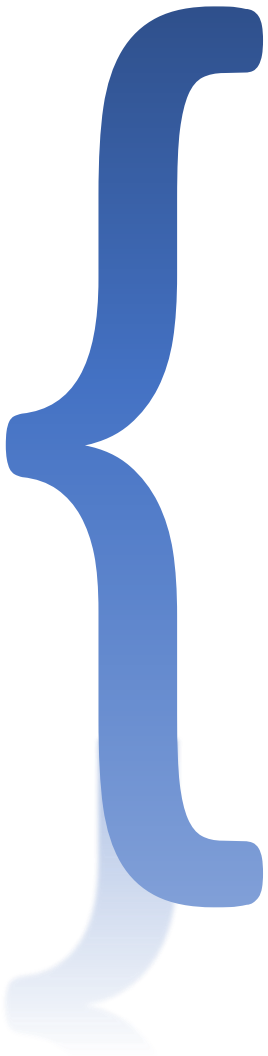

Observational cosmology

The Large-Scale Structure of the Universe

- *Slices through the 3-dimensional map of the distribution of galaxies from the Sloan Digital Sky Survey (SDSS).*
- *The Earth is at the center; each point represents a galaxy (~ 10^{11} stars each).*
- *The position of that point indicates its location in the sky, and the distance from the center of the image indicates its distance from the Earth.*
- *Galaxies are colored according to the ages of their stars, the redder are older.*
- *The outer circle is at a distance of about $2x10^{9}$ light years.*
- *The region not mapped is because dust in our own Galaxy. The lower part of the figure is thinner than the upper, thus it contains fewer galaxies.*
- *Another group completed a similar survey of the galaxies in the Universe called the 2 dF Redshift Survey.*

Credit: M. Blanton and the SDSS

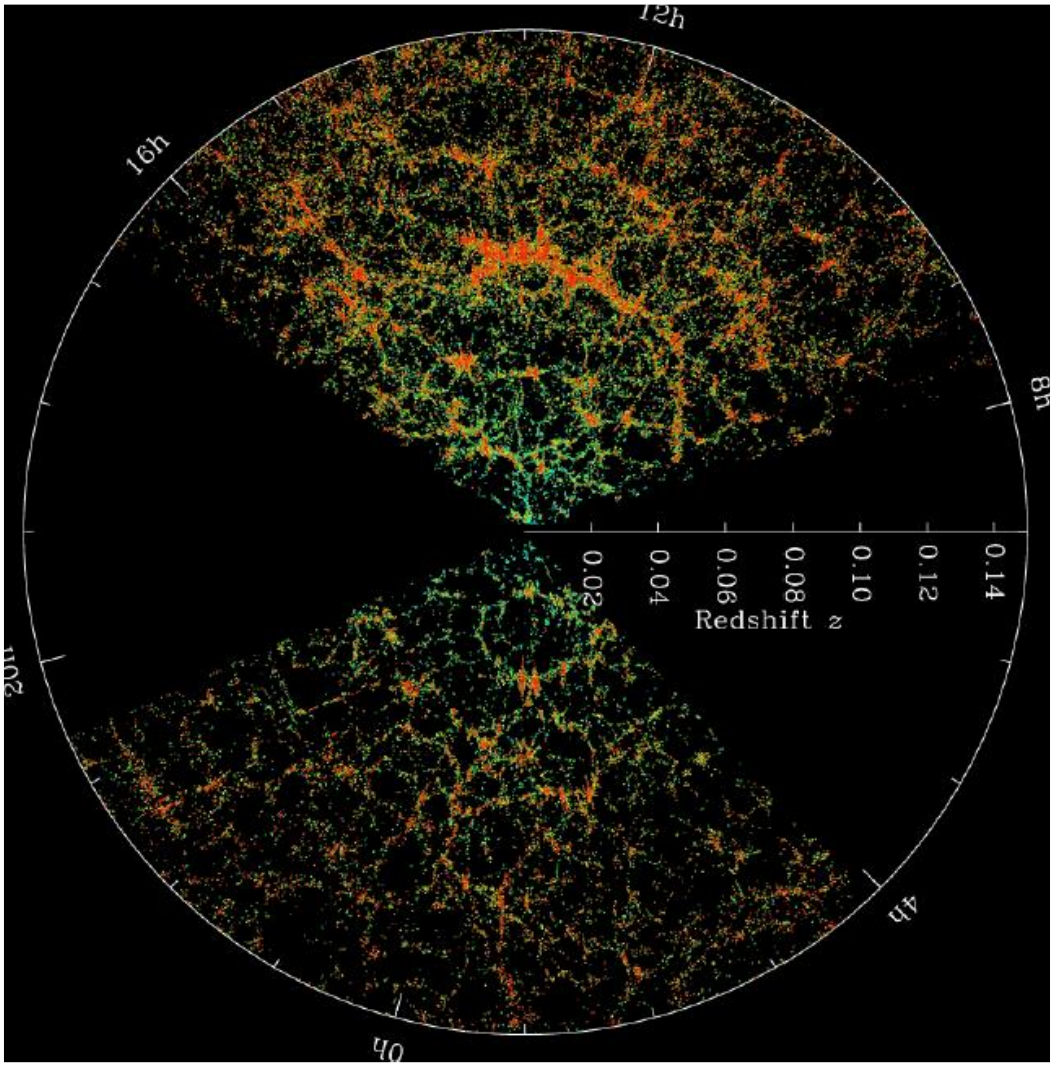

https://www.sdss3.org/science/gallery_sdss_pie2.php

Hubble's Law (I)

- **Observational cosmology** consists of the study of the structure, the evolution and the origin of the Universe through experimental measurements.
- The Hubble's observations correlate the **luminosity distance** D_L to galaxies and their velocities, measured through the **Doppler shift** (z) of the emission wavelengths.
- This shift can be measured because the emission/absorption spectra for atoms and molecules are distinctive and well known.

$$z = \frac{\lambda_{obs} - \lambda_{emit}}{\lambda_{emit}}. \quad (7.1)$$

- The discovery of **a linear relation between the z and D_L** of a Galaxy, coupled with the assumption of a linear relation between v (in km/s) and z, yields the expression for the **Hubble's Law**:

$$v = cz = H_0 \cdot D_L \quad (7.2)$$

- The Hubble constant, H_0, has physical dimensions of [time^{-1}]. Its value is

  $H_0 \sim 70$ [km/s]/Mpc

- The Hubble "constant" is a constant only in space, not in time ("0" indicates "today")
- The reciprocal of H_0 is called the ***Hubble time*** and corresponds to

  $\tau_{H0} = 1/H_0 = 13.7$ Gy.

- A plot of the luminosity distance DL vs. redshift z is usually referred to as the **Hubble diagram**. The right plot shows the deviation from the linear relation (7.2) at high z.

Hubble's Law (II)

- The **luminosity distance D_L** is defined in terms of the absolute magnitude M (i.e., intrinsic luminosity $\mathcal{L}$) and apparent magnitude m (i.e., flux $\mathcal{F}$) of objects. From the inverse-square law:

$$\mathcal{F} = \frac{\mathcal{L}}{4\pi D_L^2}$$

***Figure**: Left: Hubble diagram, i.e., the D_L of observed objects vs. their measured redshift, z. Plot based on over 1,200 Type Ia SN distance estimates (**standard candles**). For z < 0.1, we have $D_L \propto z$ yielding the Hubble relation (7.2). Right: Ratio v=cz and the velocity computed as $H_0 \cdot D_L$ on an expanded redshift scale. For large z, the Hubble law becomes nonlinear.*

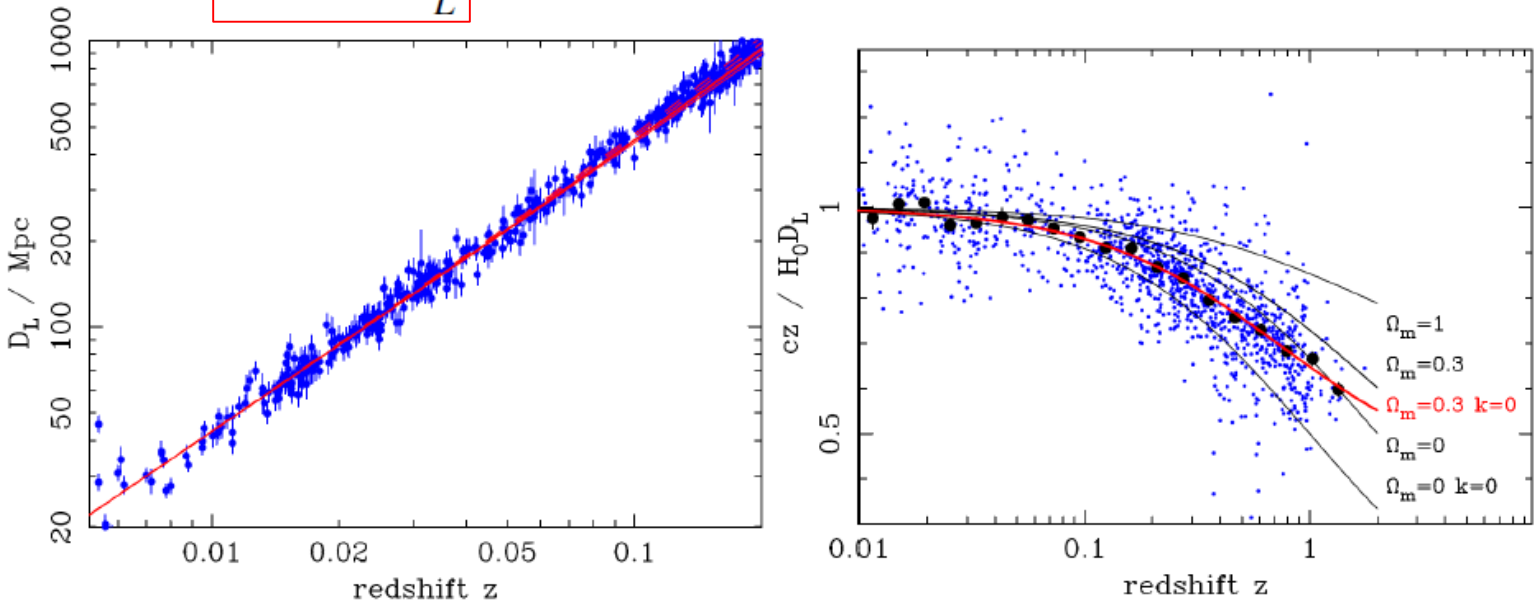

- For cosmological distances, particular care must be taken, because the D_L is **affected by relativistic effects** such as spacetime curvature, redshift and time dilation.

The Cosmic Microwave Background Radiation (CMBR)

- A second fundamental step in modern cosmology was the discovery of the CMBR, predicted in 1948 by G. Gamow and R. Alpher, as a consequence of a hot origin of the Universe.
- In 1965, A. Penzias and R. W. Wilson (Nobel Prize in 1978), discovered in a radiometer an excess of signal equivalent to a 3.5K antenna temperature.
- The COBE satellite found that the CMB has a thermal black body spectrum with

(7.4) $$E_{\rm cmb} = h\overline{\nu} \simeq 1.2 \times 10^{-3}\,{\rm eV}.$$

- The average number density of CMB photons is given by the Planck spectrum;

(7.5) $$n_{\gamma_{\rm cmb}} \simeq 400\,{\rm cm}^{-3}.$$

- The WMAP and Planck space mission improved measurements

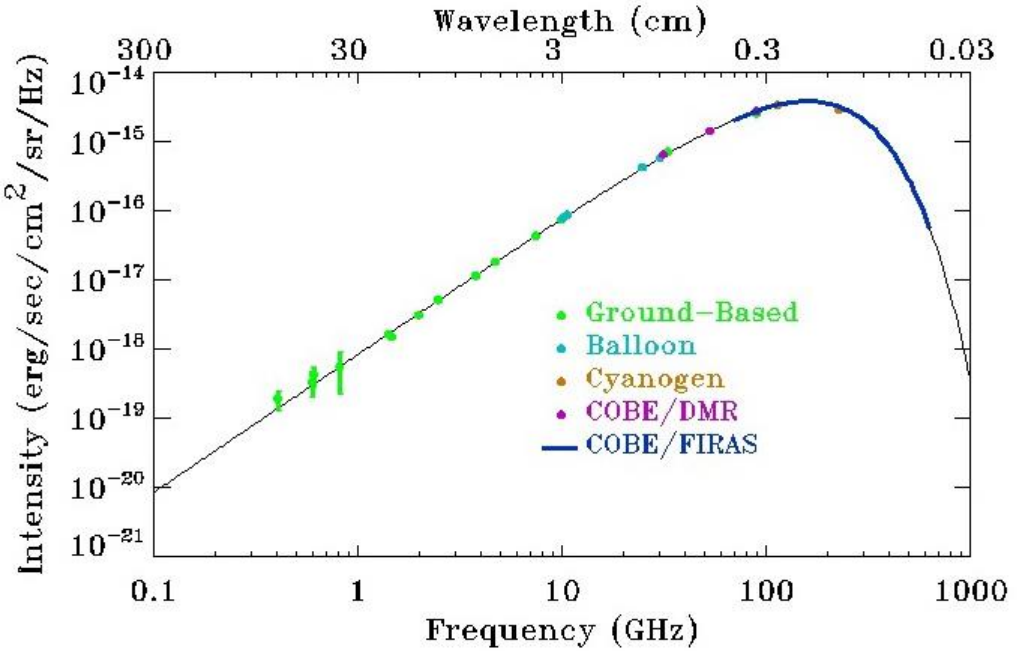

The most-precisely measured black body spectrum in nature: CMBR spectrum measured by the FIRAS on the COBE (blue points) as a function of ν and λ.

The Planck Map of CMB temperature (2018)

https://www.esa.int/Enabling_Support/Operations/Planck

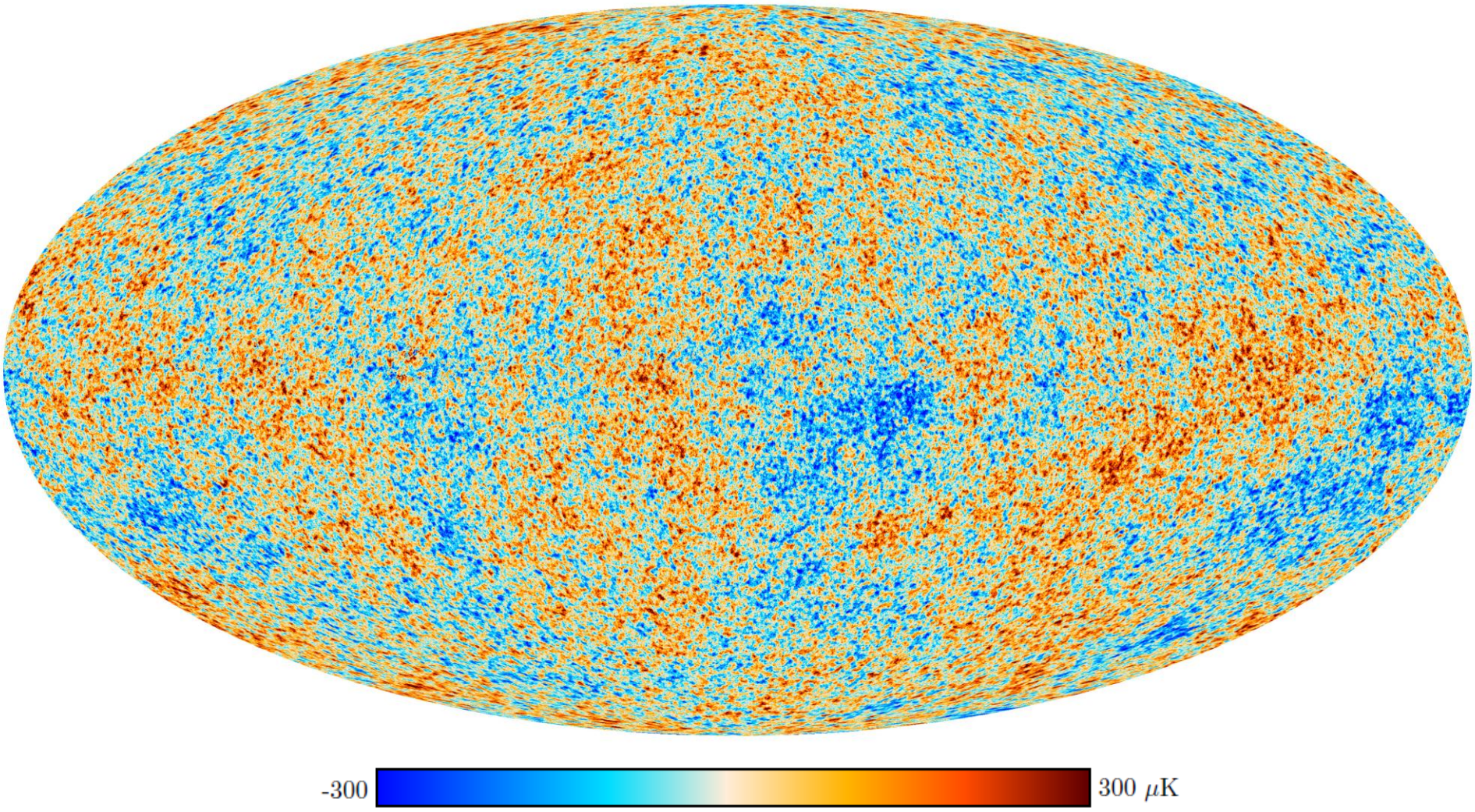

→ COSMIC HISTORY

esa

Inflation
Accelerated expansion of the Universe

Formation of light and matter

Light and matter are coupled
Dark matter evolves independently: it starts clumping and forming a web of structures

Light and matter separate
- Protons and electrons form atoms
- Light starts travelling freely: it will become the Cosmic Microwave Background (CMB)

Dark ages
Atoms start feeling the gravity of the cosmic web of dark matter

First stars
The first stars and galaxies form in the densest knots of the cosmic web

Galaxy evolution

The present Universe

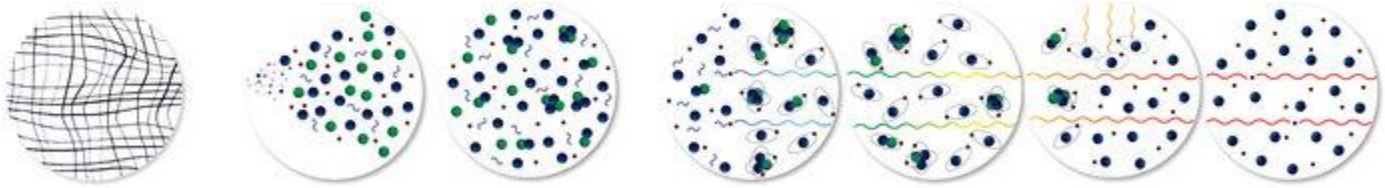

- Tiny fluctuations: the seeds of future structures
- Gravitational waves?

Frequent collisions between normal matter and light

As the Universe expands, particles collide less frequently

Last scattering of light off electrons
→ Polarisation

The Universe is dark as stars and galaxies are yet to form

Light from first stars and galaxies breaks atoms apart and "reionises" the Universe

Light can interact again with electrons
→ Polarisation

https://arxiv.org/pdf/1807.06209.pd

Parameter	TT+lowE 68% limits	TE+lowE 68% limits	EE+lowE 68% limits
$\Omega_b h^2$	0.02212 ± 0.00022	0.02249 ± 0.00025	0.0240 ± 0.0012
$\Omega_c h^2$	0.1206 ± 0.0021	0.1177 ± 0.0020	0.1158 ± 0.0046
$100\theta_{MC}$	1.04077 ± 0.00047	1.04139 ± 0.00049	1.03999 ± 0.00089
τ	0.0522 ± 0.0080	0.0496 ± 0.0085	0.0527 ± 0.0090
$\ln(10^{10} A_s)$	3.040 ± 0.016	$3.018^{+0.020}_{-0.018}$	3.052 ± 0.022
n_s	0.9626 ± 0.0057	0.967 ± 0.011	0.980 ± 0.015
H_0 [km s^{-1} Mpc^{-1}]	66.88 ± 0.92	68.44 ± 0.91	69.9 ± 2.7
Ω_Λ	0.679 ± 0.013	0.699 ± 0.012	$0.711^{+0.033}_{-0.026}$
Ω_m	0.321 ± 0.013	0.301 ± 0.012	$0.289^{+0.026}_{-0.033}$
$\Omega_m h^2$	0.1434 ± 0.0020	0.1408 ± 0.0019	$0.1404^{+0.0034}_{-0.0039}$
$\Omega_m h^3$	0.09589 ± 0.00046	0.09635 ± 0.00051	$0.0981^{+0.0016}_{-0.0018}$
σ_8	0.8118 ± 0.0089	0.793 ± 0.011	0.796 ± 0.018
$S_8 \equiv \sigma_8(\Omega_m/0.3)^{0.5}$	0.840 ± 0.024	0.794 ± 0.024	$0.781^{+0.052}_{-0.060}$
$\sigma_8 \Omega_m^{0.25}$	0.611 ± 0.012	0.587 ± 0.012	0.583 ± 0.027
z_{re}	7.50 ± 0.82	$7.11^{+0.91}_{-0.75}$	$7.10^{+0.87}_{-0.73}$
$10^9 A_s$	2.092 ± 0.034	2.045 ± 0.041	2.116 ± 0.047
$10^9 A_s e^{-2\tau}$	1.884 ± 0.014	1.851 ± 0.018	1.904 ± 0.024
Age [Gyr]	13.830 ± 0.037	13.761 ± 0.038	$13.64^{+0.16}_{-0.14}$
z_*	1090.30 ± 0.41	1089.57 ± 0.42	$1087.8^{+1.6}_{-1.7}$

Baryon density

Cold dark matter density

Hubble's constant (km Mpc^{-1} s^{-1})

Dark energy density

Matter density

Redshift of reionization

Age of the Universe (Gy)

Redshift at decoupling

A Simple Model Involving Pulsars (Chap. 6)

- High magnetic fields spinning around the nonaligned axis of rotation will produce strong electric fields $\mathcal{E}$ through Faraday's law (6.1), i.e., order of:

$$\frac{\mathcal{E}}{L} = \frac{1}{c}\frac{\mathrm{d}B}{\mathrm{d}t}$$

- the maximum energy E_{max} gained from a particle passing close to a pulsar rotating with angular velocity ω_{NS} over the length $L \sim R_{NS}$ is

$$E^{\max} = \int Ze\mathcal{E}\,\mathrm{d}x = \int Ze\frac{L}{c}\frac{\mathrm{d}B}{\mathrm{d}t}\mathrm{d}x = \int Ze\frac{L}{c}\mathrm{d}B\frac{\mathrm{d}x}{\mathrm{d}t} = ZeR_{\mathrm{NS}}B\frac{\omega_{\mathrm{NS}}R_{\mathrm{NS}}}{c}\ ,$$

- Using the derived value of the magnetic field and with $(\omega_{NS}R_{NS}/c) \sim 0.1$

$$E^{\max} = ZeR_{\mathrm{NS}}B\frac{\omega_{\mathrm{NS}}R_{\mathrm{NS}}}{c} = 4.8\times10^{-10}\ [\mathrm{statC}]\times10^{6}\ [\mathrm{cm}]\times10^{11}\ [\mathrm{Gauss}]\times0.1$$
$$\simeq 5\times10^{6}\ \mathrm{erg} \simeq 3\times10^{18}\ \mathrm{eV}\ ,$$

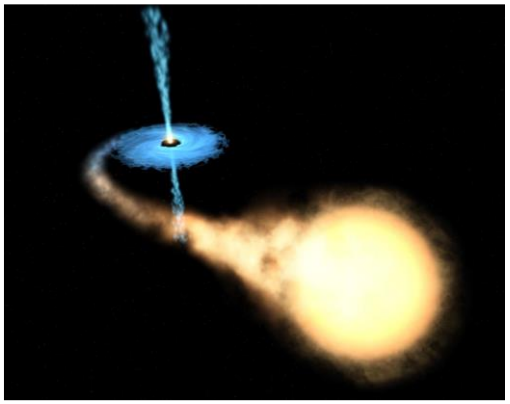

- Thus, some galactic accelerators could explain the presence of CRs with energies up to ~ 10^{18} - 10^{19} eV.
- A similar model holds for **microquasars** (binary systems, see § 6.9.2)

The Quest for Extragalactic Sources of UHECRs

- The extragalactic acceleration mechanisms must satisfy the following criteria:
  - must provide enough energy to reach the largest observed energies;
  - the accelerated population should have an injection energy spectrum that fit the observed UHECR spectrum after propagation.
- Generic models of acceleration from "Faraday law": $\boldsymbol{E_{max} = ZeLB(\frac{v}{c})}$

Ingredients:

1. Charged particles, Ze

2. Magnetic fields, B

3. Acceleration regions, L

- Electric fields through the Faraday law that can supply a consequent amount of energy: the E^{max} of a CR of charge Ze, accelerated in a region where the magnetic **field B** changes in a **spatial region of size L** is (see previous page):

$$\frac{E^{\max}}{Ze\beta} = LB. \qquad (7.8)$$

- The (7.8) can be written more appropriately as:
- Using the conversion from erg to eV:

$$E^{\max} = Z\beta\,(4.8\times10^{-10})\cdot(10^{-6})\left(\frac{B}{1\,\mu\mathrm{G}}\right)\cdot(3.1\times10^{21})\left(\frac{L}{1\mathrm{kpc}}\right)[\mathrm{erg}]. \qquad (7.9)$$

The Hillas Plot

$$E^{\max} \simeq Z\beta \cdot \left(\frac{B}{\mu\mathrm{G}}\right) \cdot \left(\frac{L}{\mathrm{kpc}}\right) \quad [\mathrm{EeV}]. \qquad (7.10)$$

- Eq. (7.10) defines the Hillas criterion for CR sources
- In the figure, several possible galactic and extragalactic acceleration sources are considered. Among them:
  - AGN
  - Gamma Ray Bursts (GRBs)
  - Magnetars

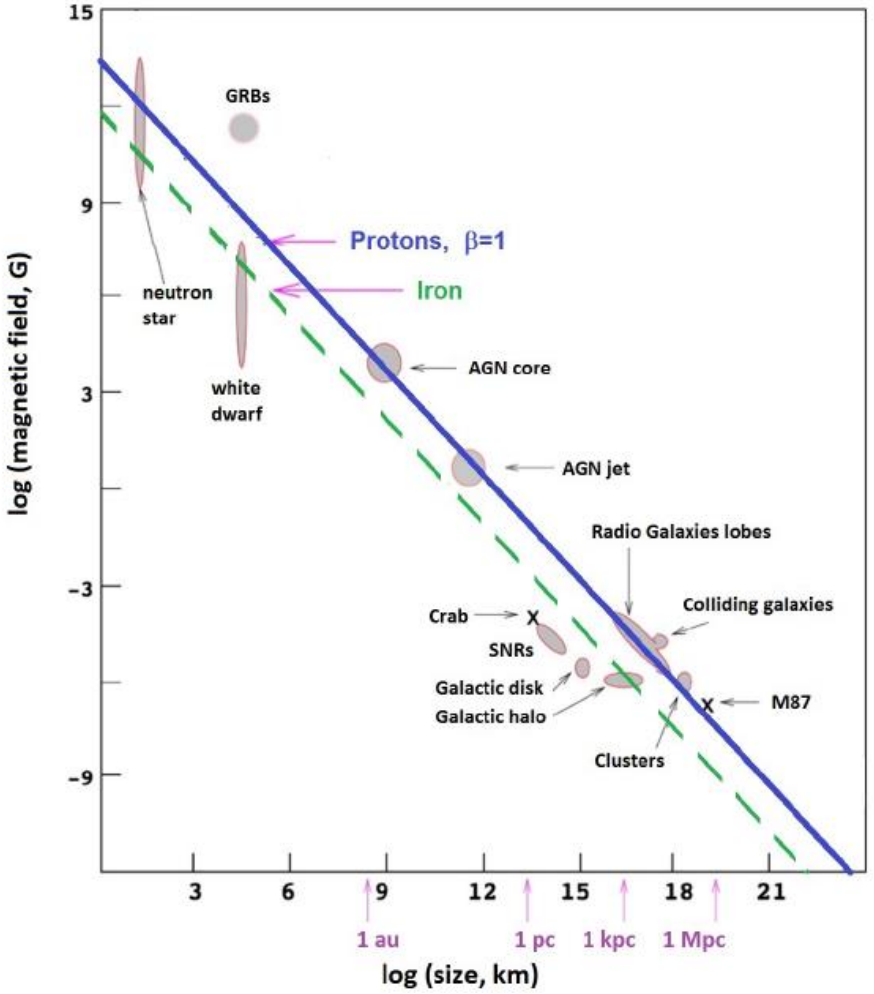

*Example of the **Hillas plot**. Acceleration of CRs up to a given energy requires magnetic fields and sizes above the respective line. The full (dashed) line corresponds to the condition for B,L to accelerate protons (iron) at 10^{20} eV. Some source candidates are still controversial*

Energy loss of UHECRs in propagation

- There are three main energy loss processes for protons (or heavier nuclei) propagating over cosmological distances:
  - adiabatic energy loss,
  - pion-production on photons of the CMBR
  - electron-positron pair-production on the CMBR
- We can define the **energy loss length** ℓ as

$$\ell^{-1} \equiv \frac{1}{E}\frac{\mathrm{d}E}{\mathrm{d}x} \,. \qquad (7.11)$$

- The quantity depends on the primary energy (apart for adiabatic eloss)

The Adiabatic Energy Loss

- The **adiabatic loss** of a CR with energy E is a general mechanism that affects particles and radiation and is due to the expansion of the Universe

$$-\frac{1}{E}\frac{\mathrm{d}E}{\mathrm{d}t} = H_0 . \quad \text{and thus} \quad \ell_{\mathrm{adia}} = \frac{c}{H_0} \simeq 4 \ \mathrm{Gpc}$$

The Propagation in the CMB: The GZK Cut-Off

- The CMB has an effect on the propagation of UHECRs
- This was studied in 1966 by K. Greisen, V. Kuzmin, and G. Zatsepin (the GZK effect or GZK cut-off).
- **GZK cut-off**: CRs protons originating at cosmological distances would be attenuated above a threshold $E_{GZK} \cong 5\ 10^{19} eV$.
- Nuclei of mass A starts to be attenuated at an energy $A \cdot E_{GZK}$.
- Protons interact with CMB photons (γ_{cmb}) if the proton energy is large enough to achieve the resonant production of the Δ^+ in the c.m. system
- The Δ^+ immediately decays; the π^0 decay in two photons, while the π^+ decays into $\mu+\nu_\mu$.

$$p + \gamma_{\rm cmb} \rightarrow \Delta^+ \rightarrow \pi^+ n \qquad (7.14)$$
$$\rightarrow \pi^0 p\ . \qquad (7.15)$$

- The neutron decays (β^-) yielding a p. As a proton is always present in the final state, the effect of the interaction is that the energy of the CR proton above threshold is reduced and **high-energy photons and neutrinos** are produced.
- The energy loss length ℓ (7.11) corresponds to (y = fraction of energy lost per interaction):

$$\ell_{p\gamma}^{-1} = \langle y \sigma_{p\gamma} n_\gamma \rangle \quad \longrightarrow \quad \ell_{p\gamma} \equiv \frac{1}{\langle y \sigma_{p\gamma} n_\gamma \rangle}\ , \qquad (7.16)$$

Kinematics of the GZK Cut-Off

- We derive now the **threshold energy** for protons to induce this reaction and their **mean free path**.
- The Δ^+ resonance has mass $m_\Delta = 1{,}232\,\mathrm{MeV}$
- Consider the 4-momenta of a proton $p_p = (E_p, \mathbf{p_p})$ and of a CMB photon $p_\gamma = (E_\gamma, \mathbf{p}_\gamma)$
- The Δ^+ is produced at c.m. energy $\sqrt{s} = m_\Delta$

$$s = (p_p + p_\gamma)^2 = m_\Delta^2$$
$$m_p^2 + 2E_\gamma E_p - 2\mathbf{p}_p\mathbf{p}_\gamma = m_\Delta^2. \qquad (7.17)$$

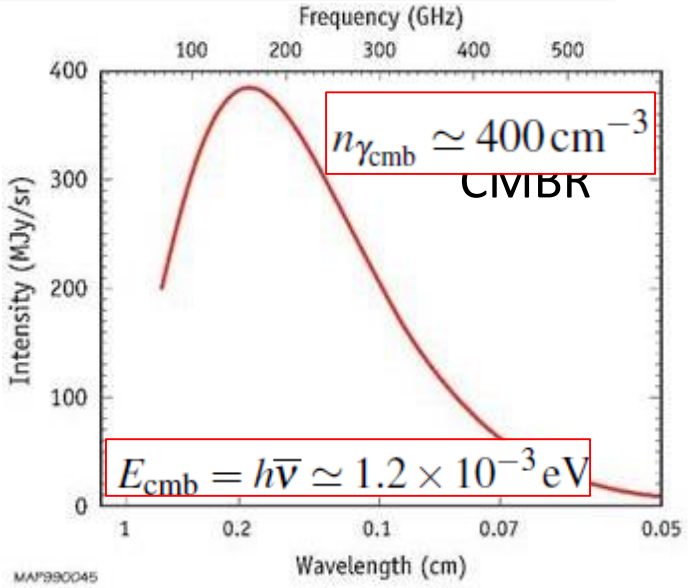

- For a photon, $|\mathbf{p}_\gamma| = E_\gamma$, and at high energy, $E_p \simeq p_p$ Thus, (7.17) becomes →

$$2E_p(E_\gamma - E_\gamma \cos\theta) = m_\Delta^2 - m_p^2$$

- Using the values of the p and Δ^+ masses

$$E_p = \frac{m_\Delta^2 - m_p^2}{2E_\gamma(1-\cos\theta)} = \frac{0.32\,\mathrm{GeV}^2}{E_\gamma(1-\cos\theta)}. \qquad (7.18)$$

- The minimum for E_p occurs when $\theta = \pi$. Then, for collision with the CMBγ with $E_\gamma = 1.2\ 10^{-3}\,\mathrm{eV}$ the threshold is

$$E_p = \frac{m_\Delta^2 - m_p^2}{4E_\gamma} = 1.2 \times 10^{20}\,\mathrm{eV}.$$

- The threshold E_p decreases when the interaction occurs with higher energy CMBγ. The **effect starts to become significant for protons with $E_p = 5\text{x}10^{19}$ eV.**

The energy loss length

$$\ell_{p\gamma} \equiv \frac{1}{\langle y \sigma_{p\gamma} n_\gamma \rangle} \qquad (7.16)$$

$$n_{\gamma_{\rm cmb}} \simeq 400\,{\rm cm}^{-3}$$

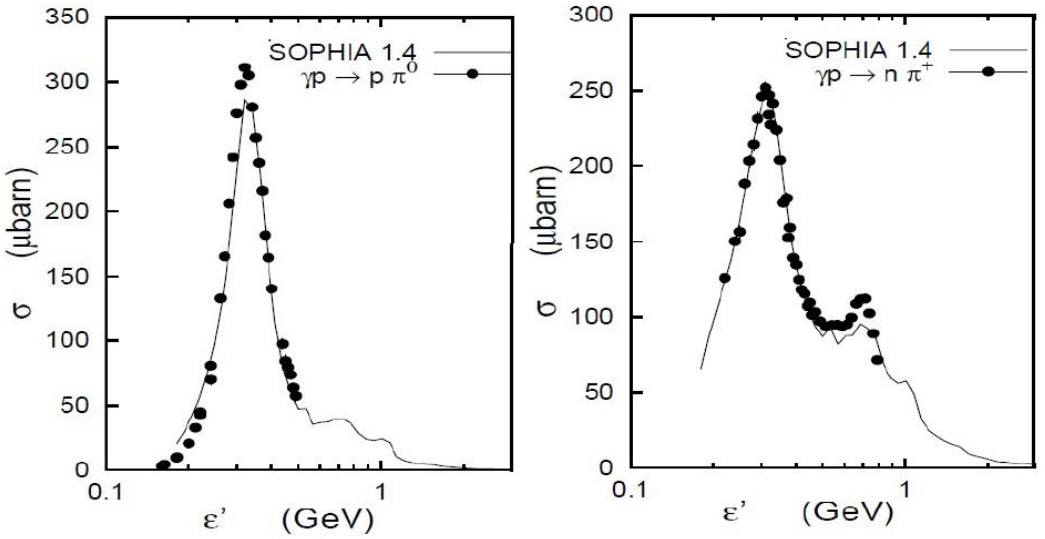

- The cross-section for Δ^+ at resonance is (see figure)

$$\sigma_{p\gamma} \simeq 250\,\mu{\rm b}.$$

- The E-loss per interaction is relatively small and can be estimated considering that, in the final state of the process, a proton and a pion are present, and thus:

$$y = \frac{\Delta E_p}{E_p} \sim \frac{m_\pi}{m_p} \simeq 0.1\ . \qquad (7.20)$$

- Within a few successive interactions, the proton energy decreases to a value below the threshold for the reaction. The energy loss length (7.16) corresponds to

$$\ell_{p\gamma} = \frac{1}{y \cdot \sigma_{p\gamma} \cdot n_{\gamma_{\rm cmb}}} = \frac{1}{0.1 \cdot 250 \times 10^{-30} \cdot 400} = 10^{26}\,{\rm cm} = 30\,{\rm Mpc}.$$

- All protons originating at D>30 Mpc arrive on Earth with energy below 10^{20} eV.
- **This horizon is small in terms of the dimensions of the Universe**.

Proton energy losses vs. E

- During the propagation in the CMB, e+e- pairs can be also produced in the process

$$p + \gamma \rightarrow p + e^+ e^- .$$

- The energy loss lengths for this process can be computed similarly to that of the GZK.
- The Figure compares the relative contributes of the three considered processes

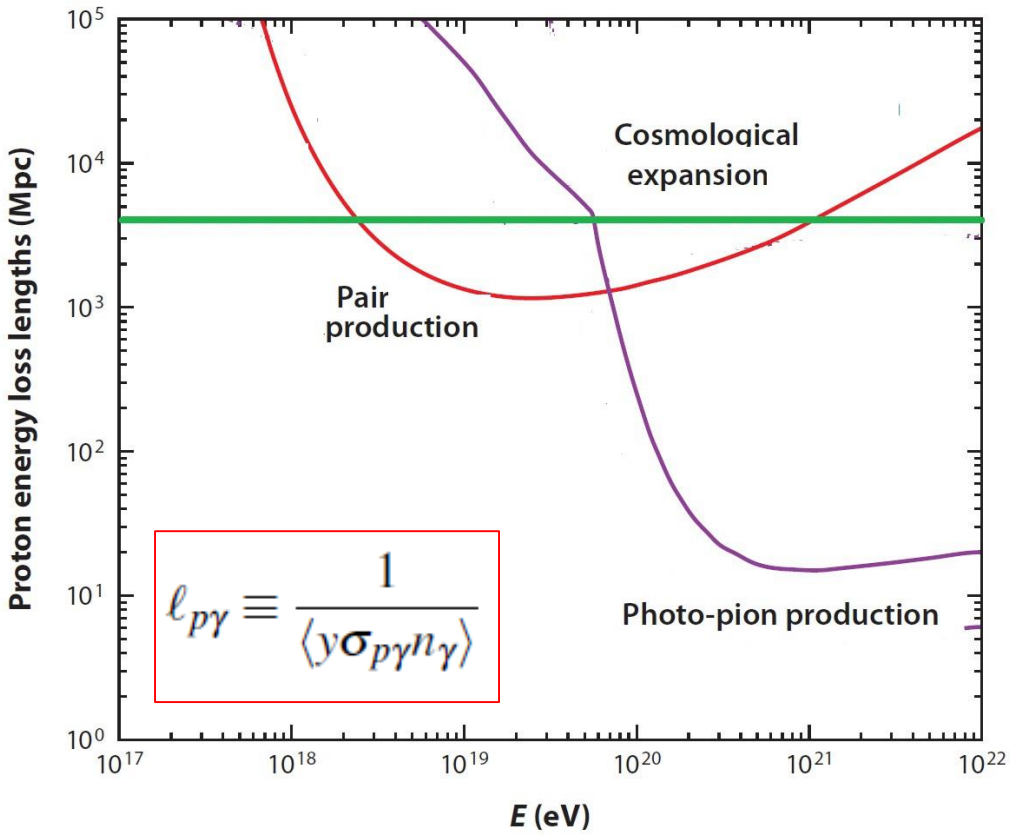

The energy loss lengths (7.16) for a high-energy proton propagating through the CMB radiation field. Pair creation, photo-pion production, and energy loss through cosmological expansion (7.13) are shown

The proton horizon

- The neighboring superclusters of galaxies (<300 Mpc)
- There are about 100 superclusters and about 3 10^6 large galaxies.
- The central sphere corresponds to 100 Mpc (>GZK limit)

- *Enjoy with a beautiful web site designed to give an idea of what our universe looks like at different scales, created by R. Powell:*

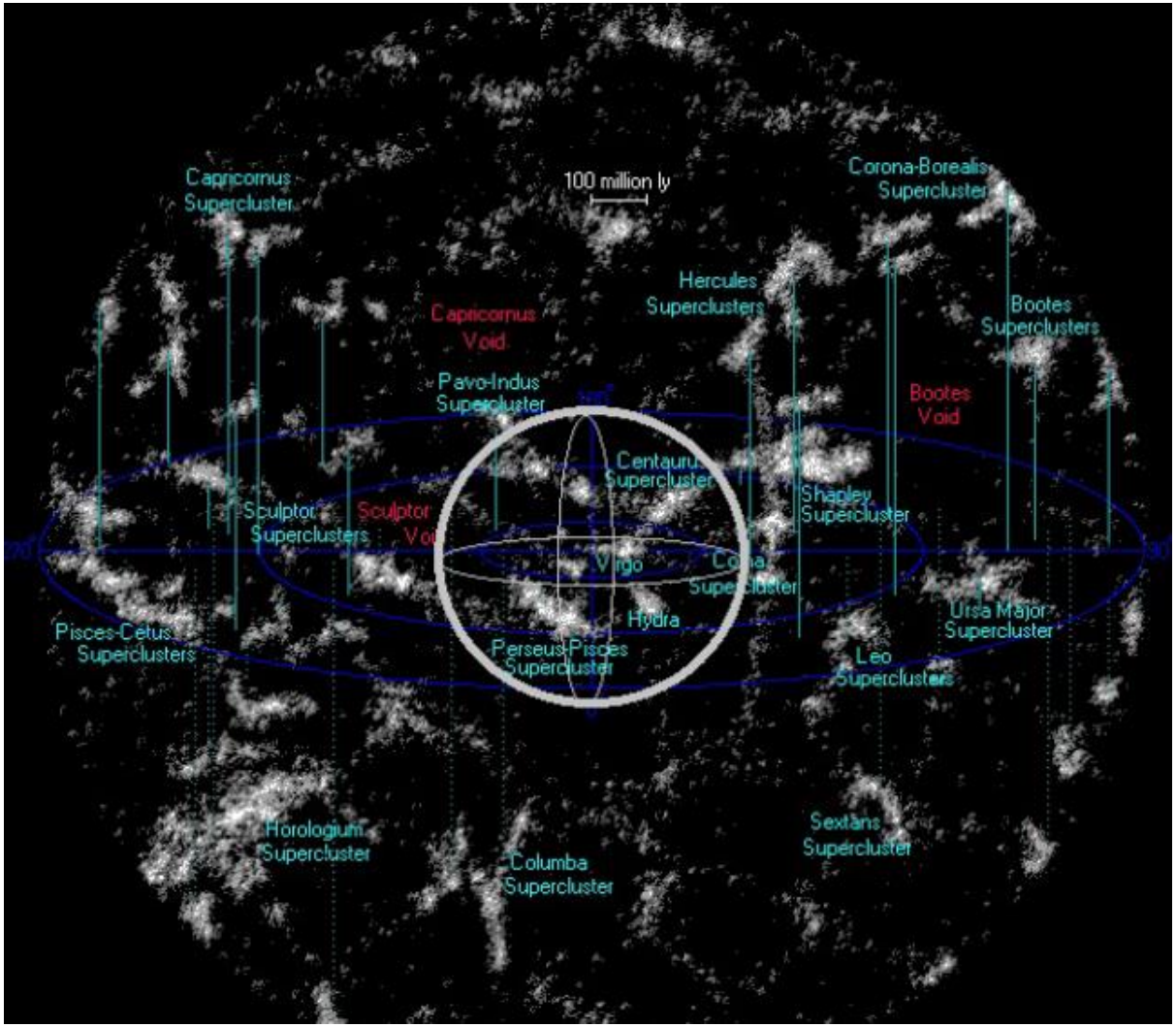

http://www.atlasoftheuniverse.com/

UHECRs detection methods: I) EAS

- **Two techniques are employed to detect UHECRs**. The first extends the use of EAS arrays (Chapter 4) to energies above 10^{18} eV.
- **AGASA** took data between 1984 and 2003. It consisted of **111** scintillation counters, each of 2.2m^2, placed at a distance of 1 km from each other and covering an effective surface of 100 km^2.

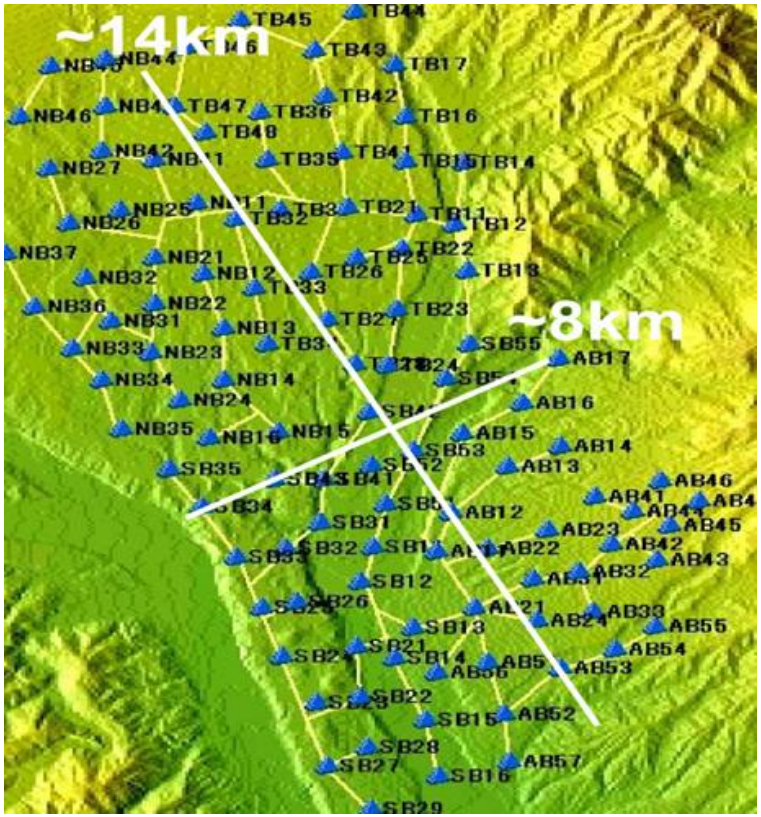

The layout of the Akeno Giant Air Shower Array (AGASA)

Our toy detector (Chap. 4)

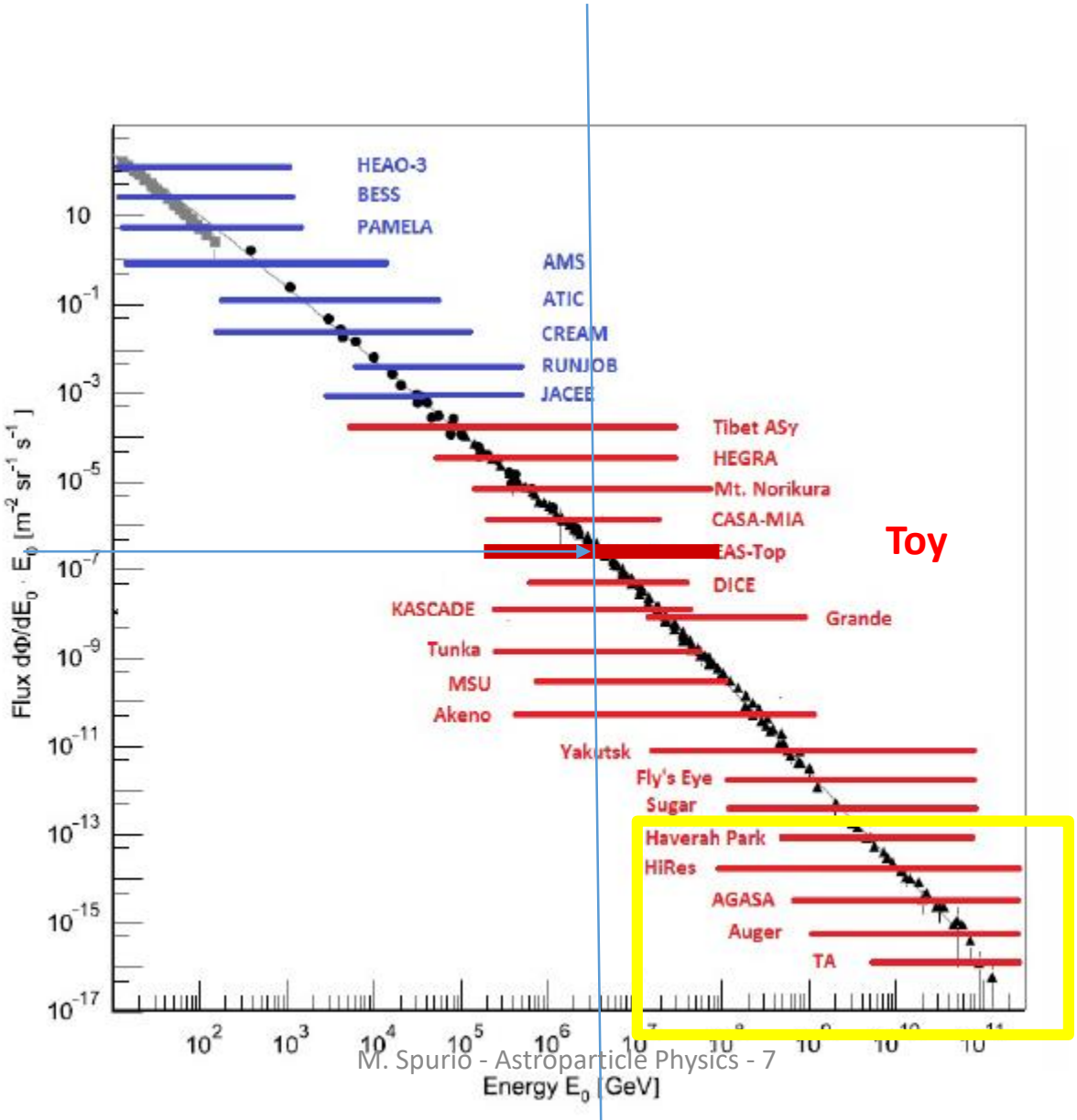

UHECRs detection methods: II) Fluorescence

- The second exploits the **excitation of nitrogen molecules** by charged particles in the shower and the associated fluorescence emission of light.
- The light is detected by photomultipliers and the profile of the shower in the atmosphere can be inferred rather directly by **ground detectors**.
- The **limitation** of this type of detectors is that **they may only operate in clear, moonless nights**. Any spurious source of light would be a problem.

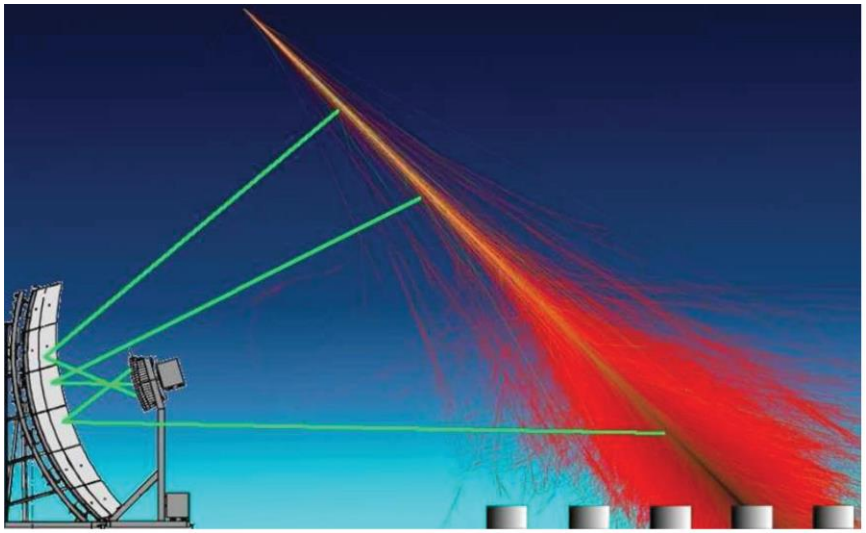

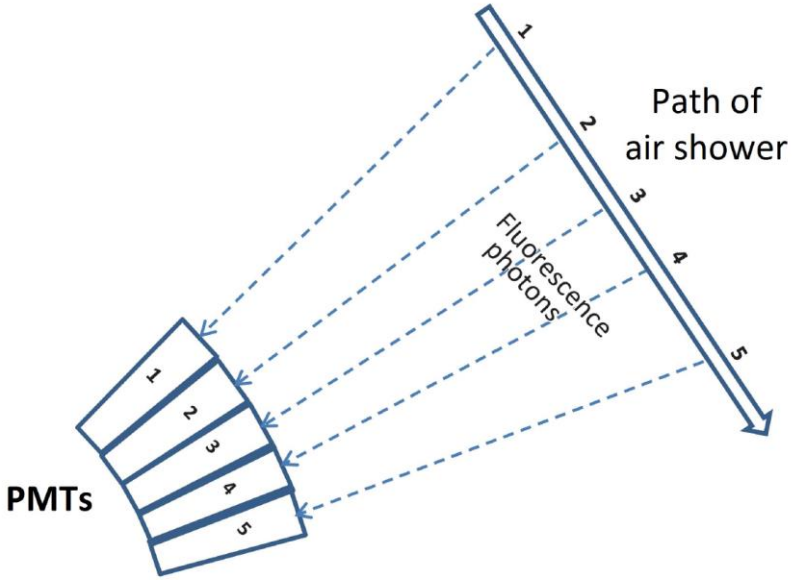

Fluorescent Light and Fluorescence Detectors

- Fluorescent emission is isotropic: the air showers can be observed from all directions
- The observations allow us to follow the development of the shower and to evaluate the position of maximum in the atmosphere, X_{max}.
- To record the longitudinal development, many PMTs, closely packed together, pointing towards different but adjacent regions are used.

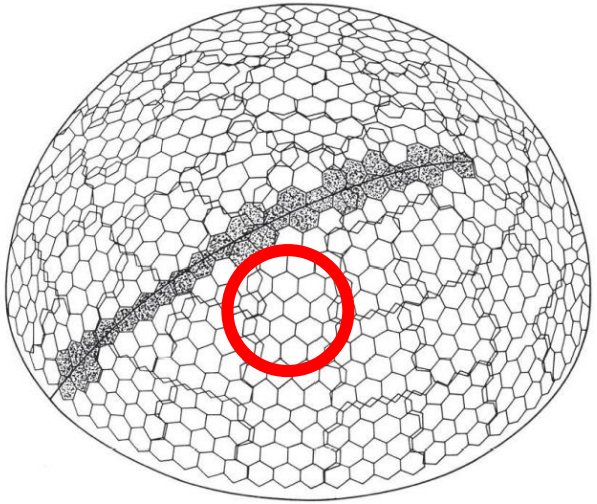

One of the 67 PMTs in the Fly's Eye experiment and the layout

High Resolution Fly's Eye detector (HiRes), (Utah)

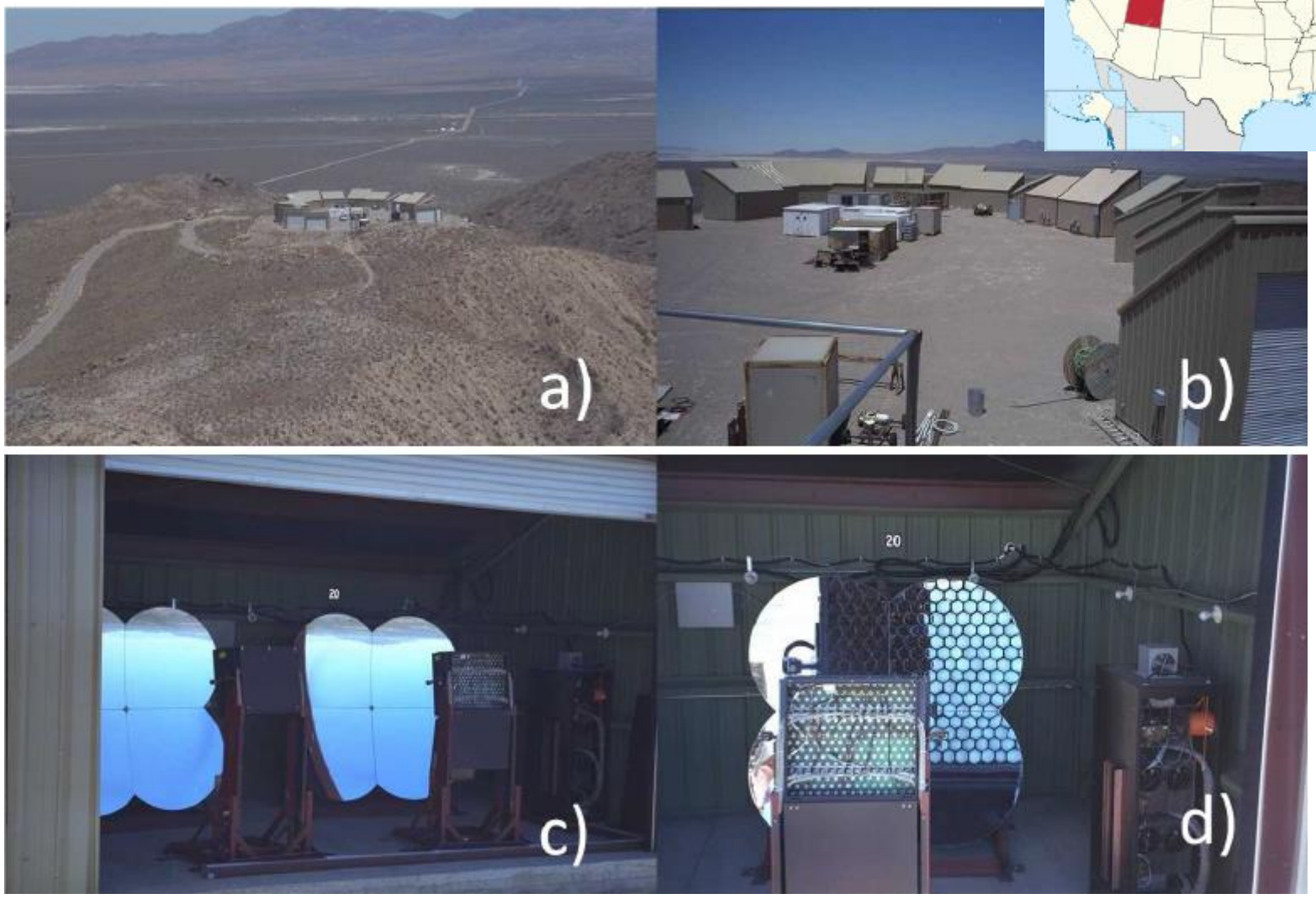

Detection principles of a fluorescence detector

- Fluorescence detectors use large spherical mirrors to improve light collection.
- The light is then focused on an array of small PMTs.
- Whit only one array, ambiguous solutions can be found. If more than one telescope is available, each telescope provides its own shower-detector plane, and the geometry of the shower axis is constrained to within a fraction of a degree.
- This technique, first used by **HiRes**, is known as **stereo reconstruction**.
- Another possibility is to complement the fluorescence detector with a surface shower detector. This independently provides the position of the impact point of the shower on the ground.
- This, known as the **hybrid technique**, used in both the Pierre Auger Telescope Array experiments.

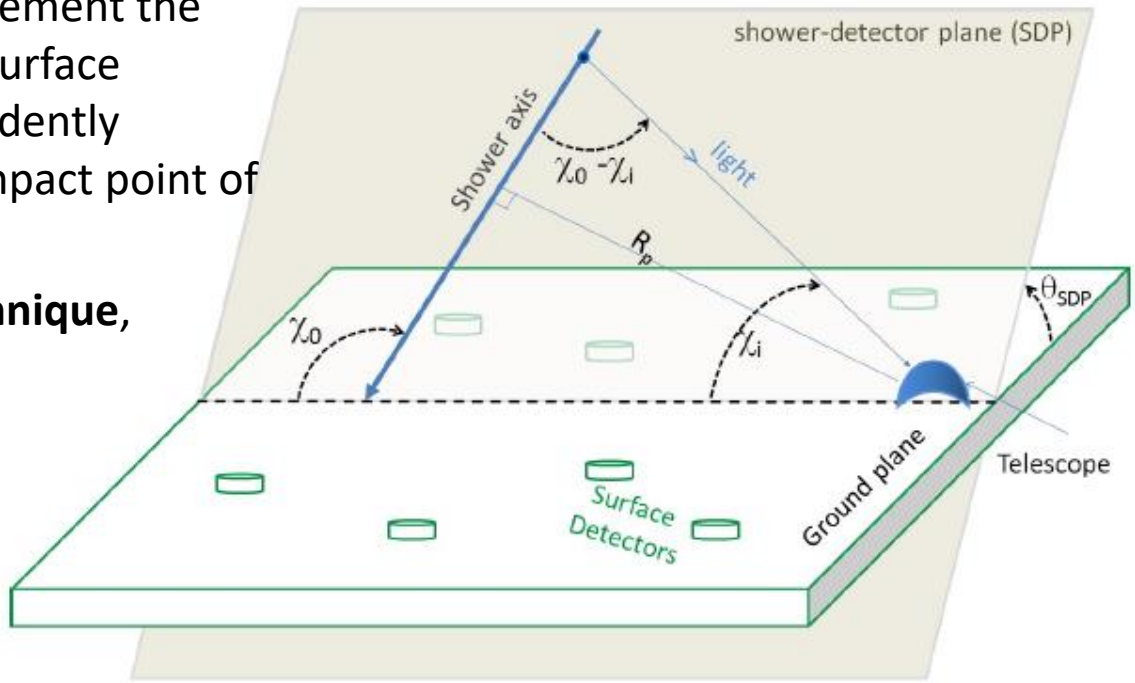

The highest energy HiRes stereo event

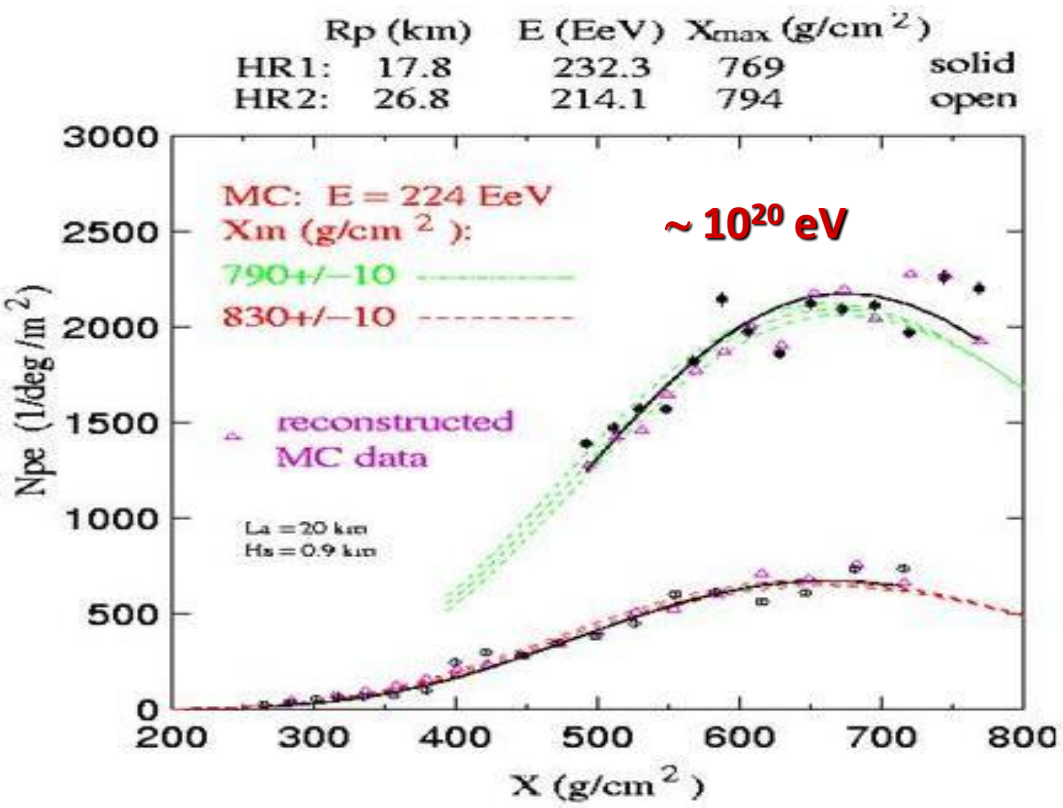

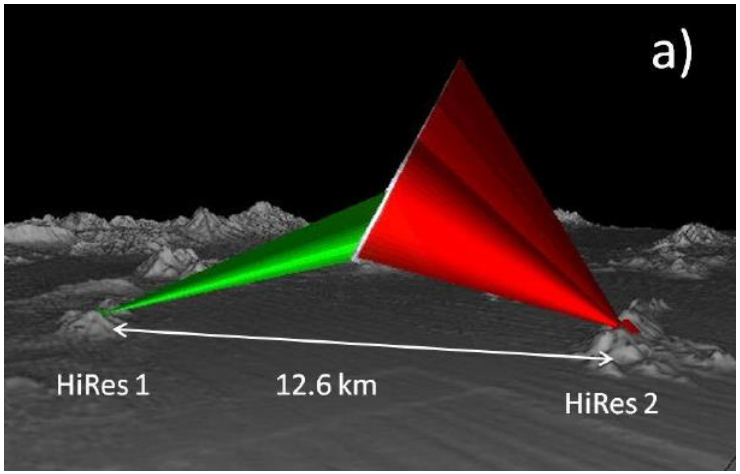

- *Note: this event has a reconstructed energy >10^{20} eV. After calibration, the total energy is slightly reduced below 10^{20} eV (see figure next page)*

Experimental status before 2007

- **HiRes** results were compatible with no events > 10^{20} eV, in agreement with the GZK
- **AGASA** has observed 11 events above 10^{20} eV with zenith<45°.

- Differently from HiRes, AGASA results seemed to indicate that the energy spectrum continues without discontinuity beyond $5x10^{20}$ eV, in violation of the GZK effect
- One possible explanation for the discrepancy between the two experiments is **a possible bias regarding the energy assignment** of the parent CR from one (or both) of the two methods.
- The use of hybrid detectors was mandatory → PAO and TA

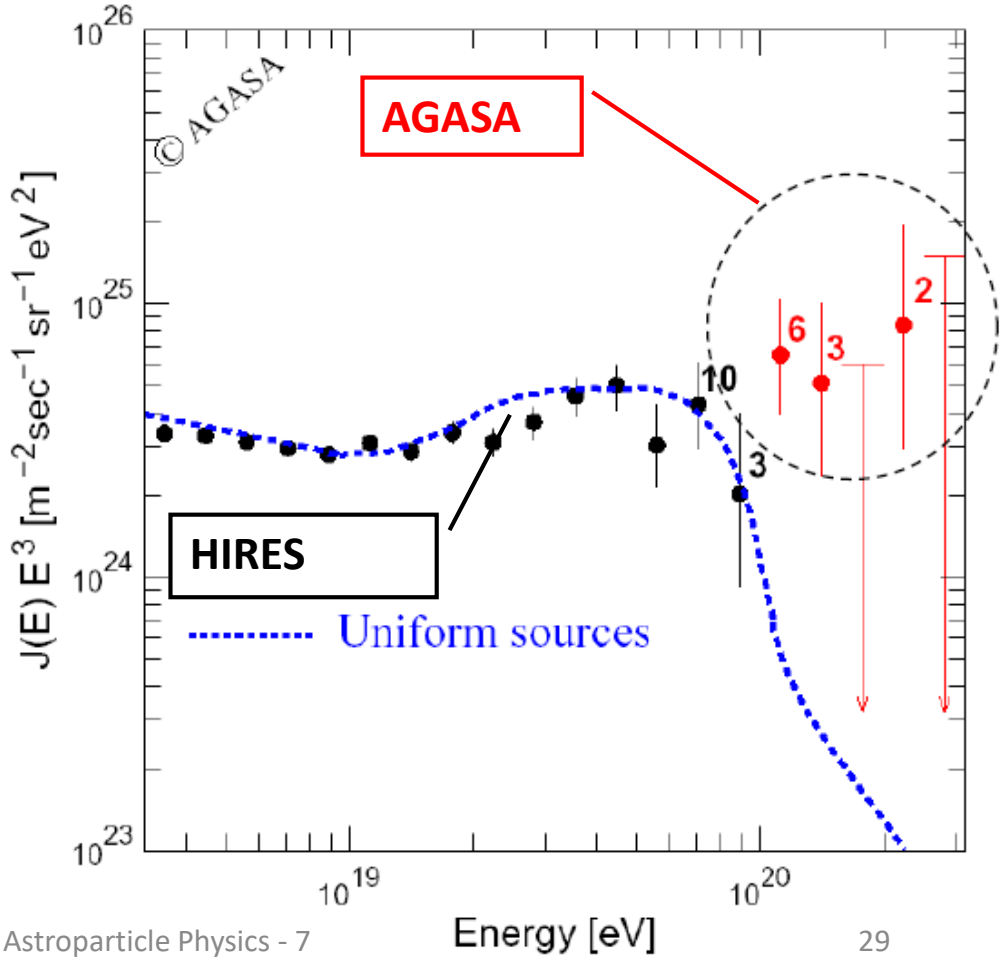

The Pierre Auger Observatory (PAO)- 2008→

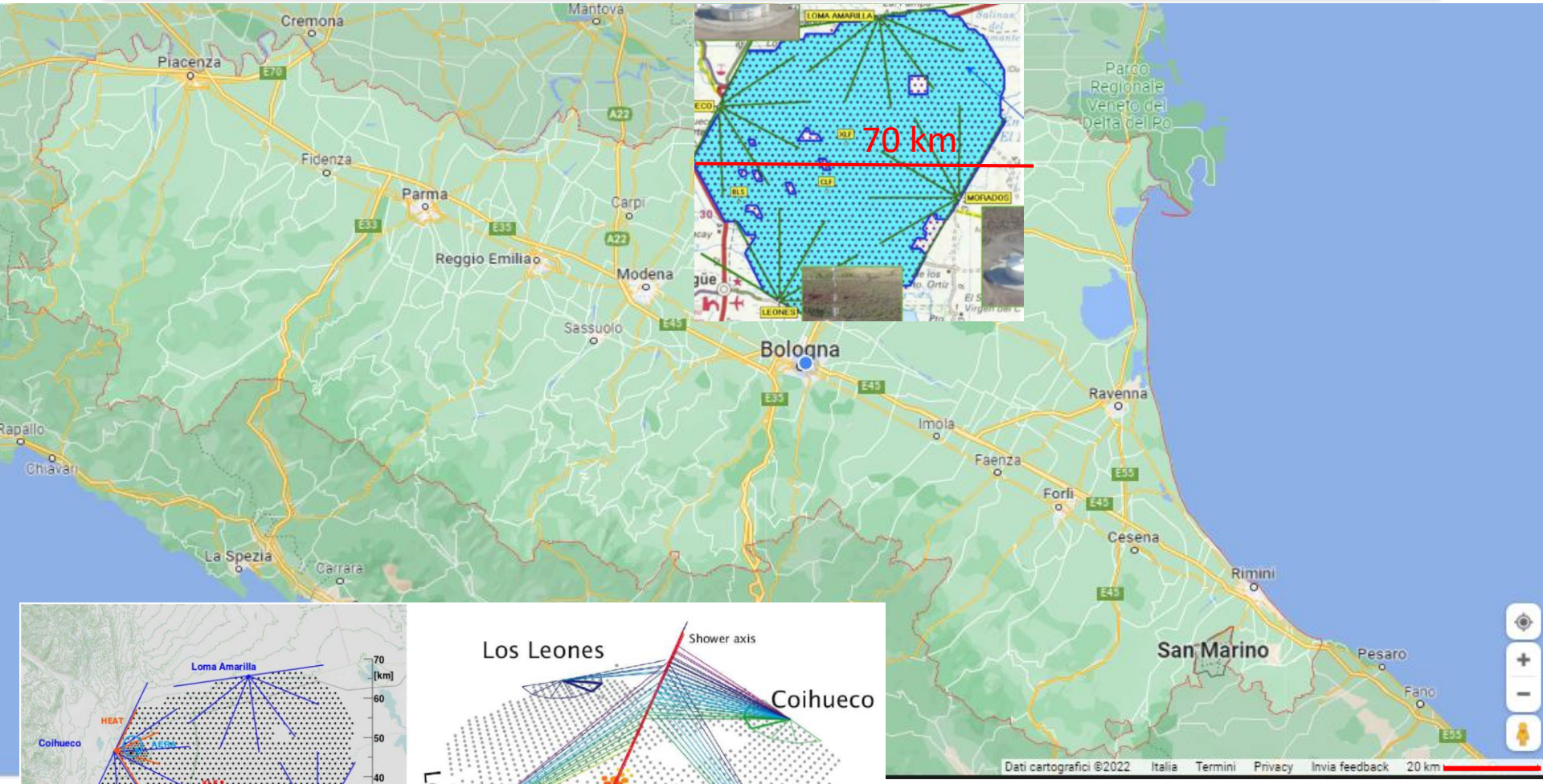

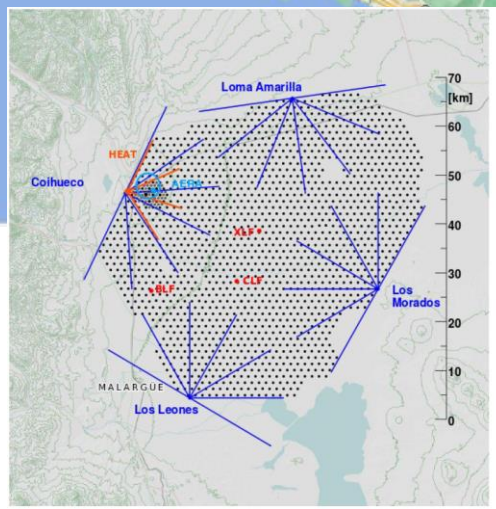

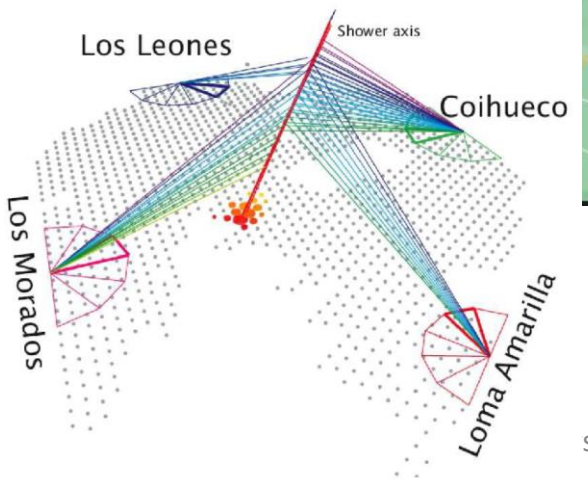

PAO


Stati Uniti
Ocean Atlantico settentrionale
Messico
Golfo del Messico
Cuba
Porto Rico
Guatemala
Mar dei Caraibi
Nicaragua
Venezuela
Guyana
Colombia
Suriname
Ecuador
Brasile
Perù
Bolivia
Hotel Alejandro I
Cile
Uruguay
Argentina
Google

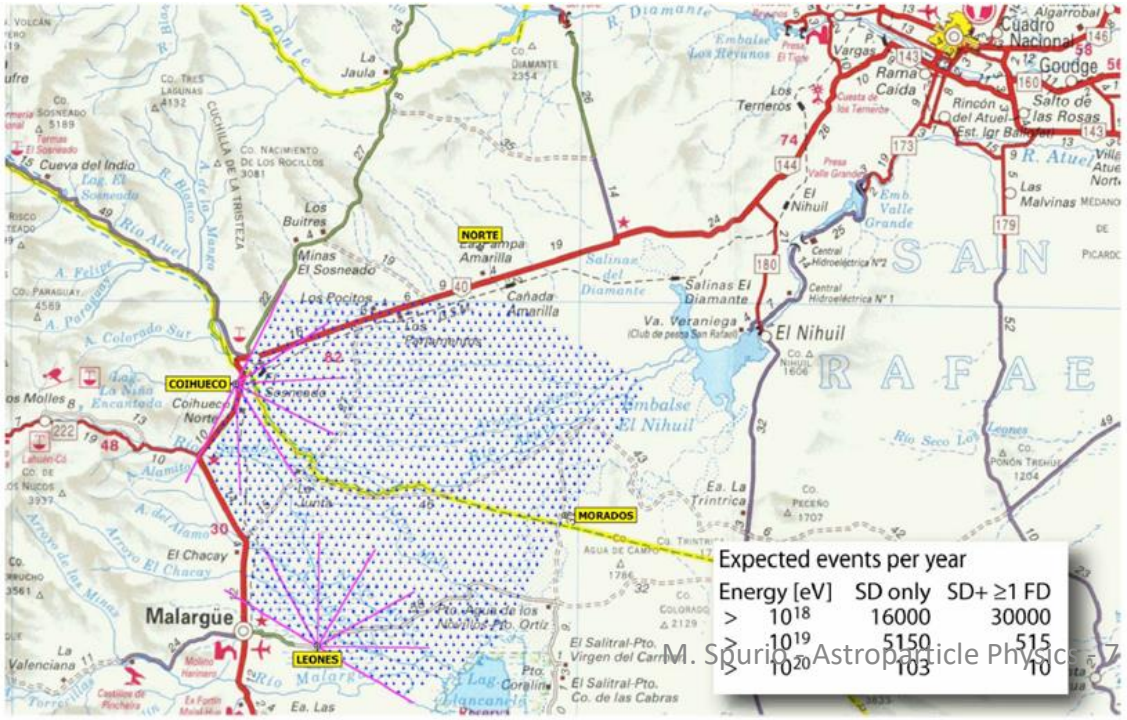
NORTE
COIHUECO
MORADOS
LEONES
Malargüe
Cuadro Nacional
Goudge
Salto de las Rosas
El Nihuil
Expected events per year
Energy [eV] SD only SD+ ≥1 FD
> 10^18 16000 30000
> 10^19 5150 515
> 10^20 103 10


REPÚBLICA DE BOLIVIA
REPÚBLICA DEL PARAGUAY
JUJUY
SALTA
CHACO
CATAMARCA
TUCUMÁN
SANTIAGO DEL ESTERO
CORRIENTES
LA RIOJA
SAN JUAN
CÓRDOBA
SANTA FE
ENTRE RÍOS
MENDOZA
BUENOS AIRES
LA PAMPA
NEUQUÉN
RÍO NEGRO
CHUBUT
SANTA CRUZ
TIERRA DEL FUEGO, ANTÁRTIDA E ISLAS DEL ATLÁNTICO SUR
Ushuaia
Río Gallegos
Islas Malvinas (Arg.)
OCÉANO PACÍFICO SUR
OCÉANO ATLÁNTICO SUR
CORDILLERA DE LOS ANDES
REPÚBLICA DE CHILE
1-Límite del lecho y subsuelo
2-Límite exterior del Río de la Plata
3-Límite lateral marítimo argentino-uruguayo

The Pierre Auger Observatory (PAO)

- The Pierre Auger Observatory (PAO) was completed in 2008.
- The layout of the PAO consists of a **surface detector (SD) array,** with 1,600 water Cherenkov detectors spaced by 1.5 km on a grid covering an area of 3,000 km^2.
- Each **tank of the SD array** has a 10m^2 surface and 1.2m depth of purified water. Each station is equipped with three PMTs to measure the Cherenkov light and:

- Flash Analog to Digital Converters (FADC),
- electronic cards for control and trigger,
- a solar panel and two batteries for power,
- a GPS receiver for the time tagging,
- a custom radio emitter and receiver for trigger and data transfer.

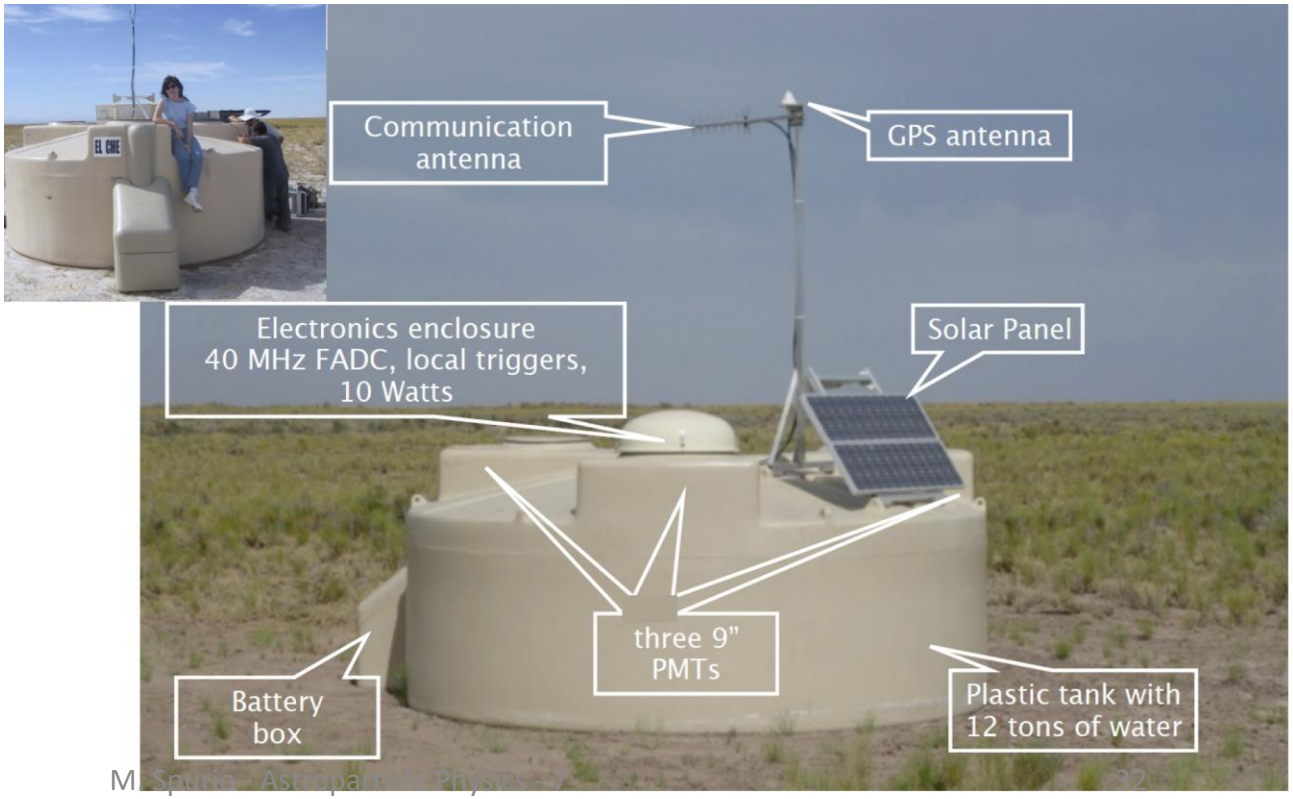

The Surface Detector (SD) Array (particular)

The Surface Detector (SD) Array of PAO

- The SD has a 100% duty cycle and the height of the individual SD tanks allows to detect muons with also excellent sensitivity to horizontal showers.

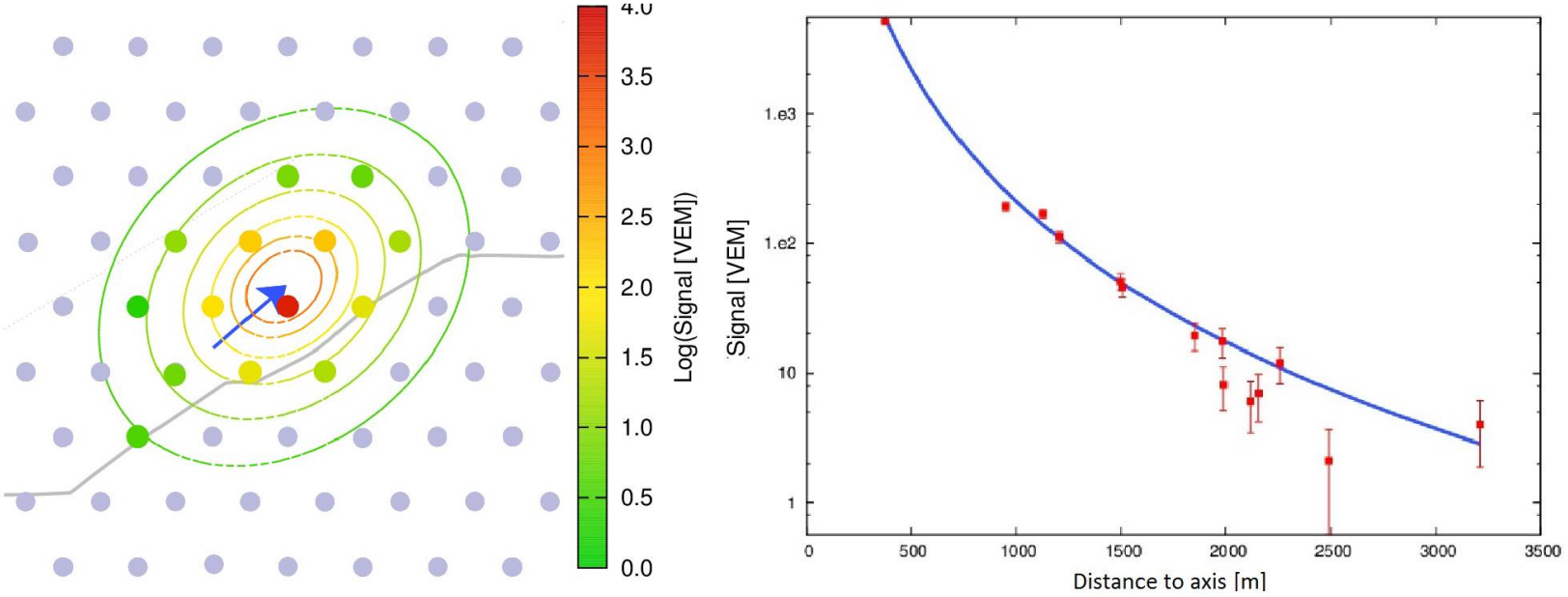

- *Left: zoomed view of the PAO SD interested by a cascade. The quantity is expressed in terms of a vertical equivalent muon (VEM) crossing a tank. The concentric lines represent the distance from the axis shower with an equal number of particles, obtained after reconstruction.*
- *Right: fit of the event using the Auger Lateral Distribution Function. On the y-axis, the signal in units of VEM is proportional to the signal density ρ = particles/cm^2 vs. the distance from the axis shower.*

The Fluorescence Detector (FD) of the PAO

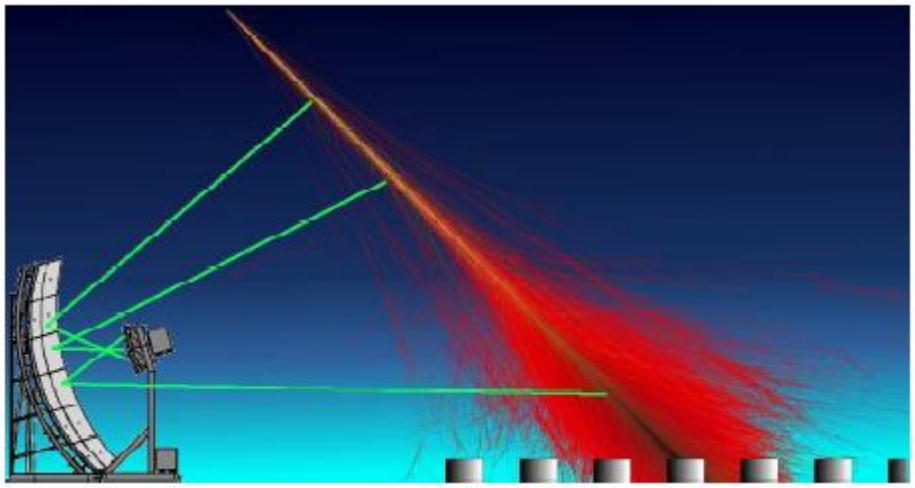

- The PAO uses four sites, "eyes".
- Their geometrical arrangement ensures full detection efficiency for showers from primaries with E > 10^{19} eV over the entire surface of the array.
- The primary CR energy is determined by the FD in a calorimetric way using the reconstructed energy deposited along the shower's profile

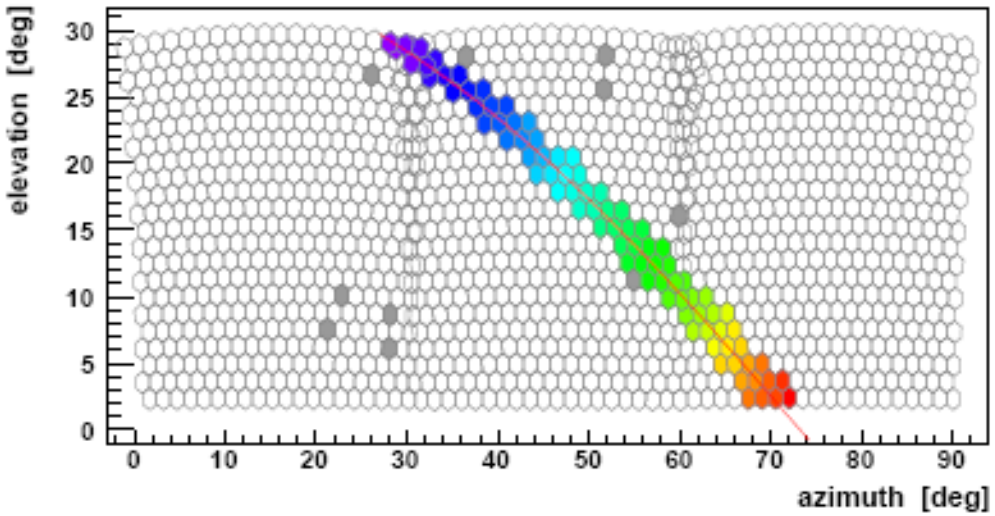

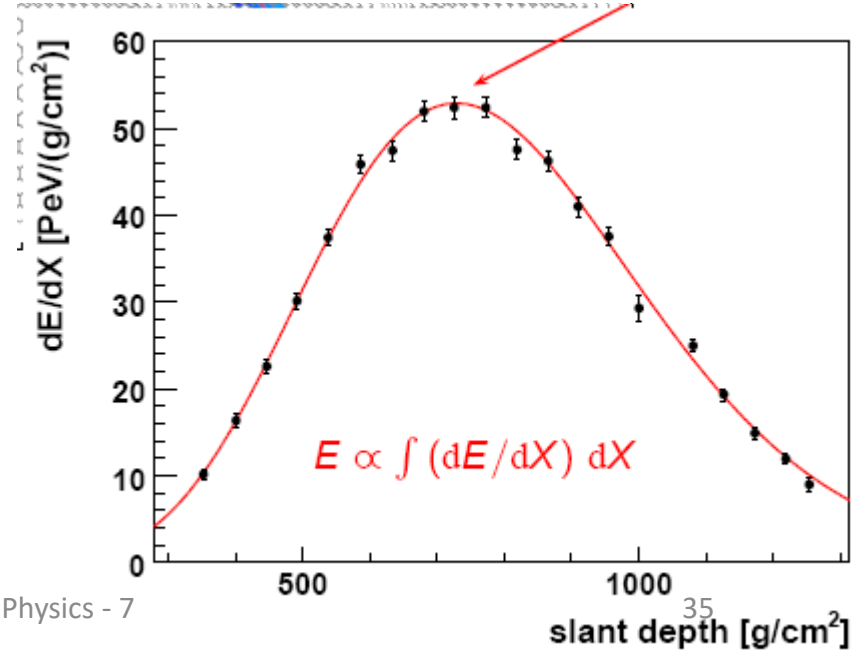

Hybrid Events

- **Energy scales**. The sub-sample of EAS recorded by both the FD and the SD is used to relate the energy reconstructed with the FD, to that used by the SD. The energy scale inferred from this data sample is applied to all showers detected by the SD array.

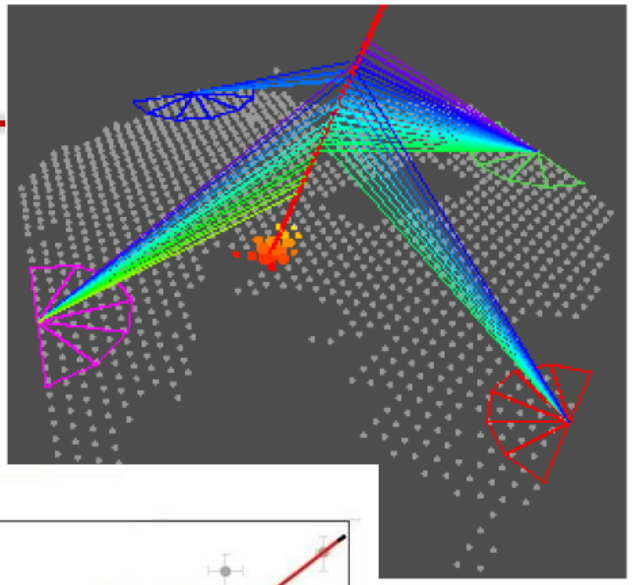

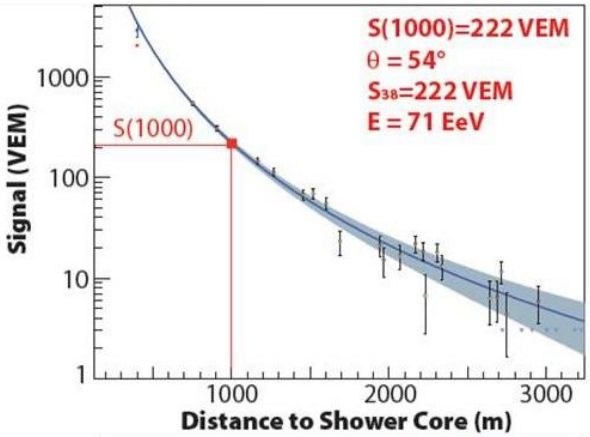

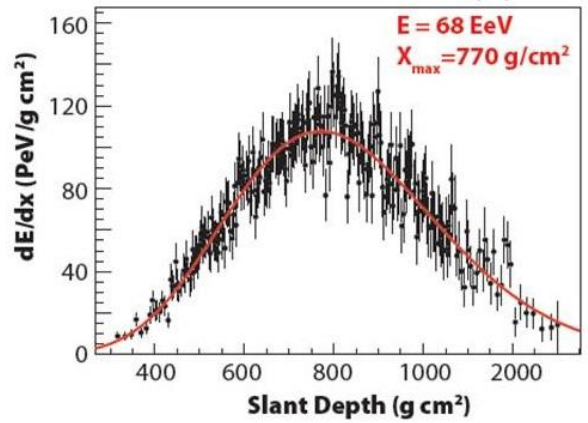

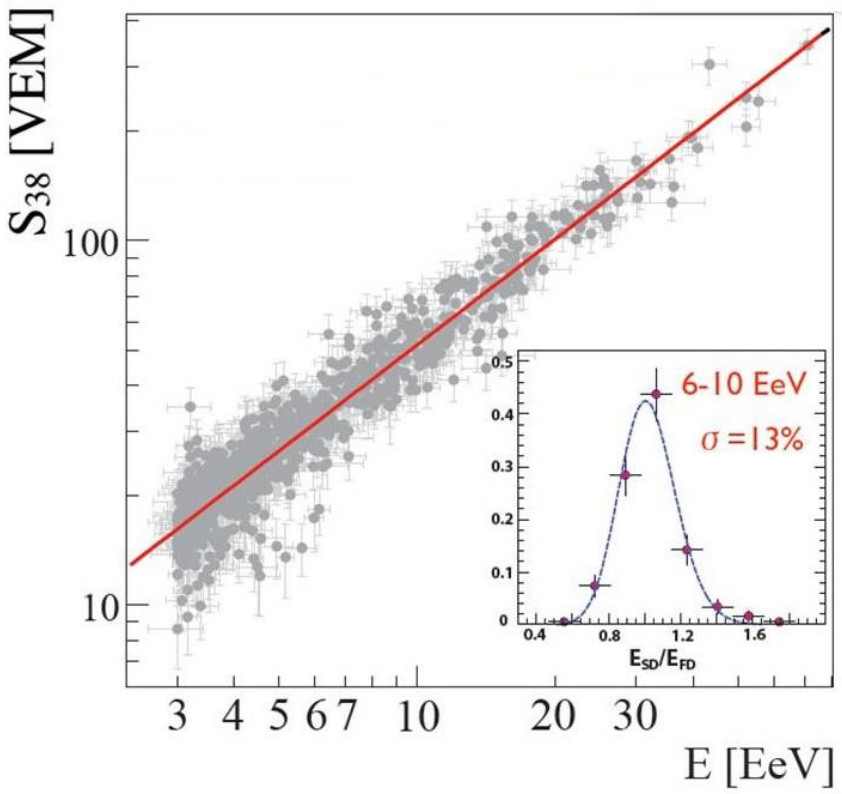

The Telescope Array (Utah)

	Pierre Auger Observatory	Telescope Array
Average latitude	35.3° S	39.4° N
Location	Mendoza, Argentina	Utah, USA
Average altitude	1,400 m	1,400 m
Surface Detectors		
Surface area	$\sim 3{,}000$ km^2	~ 760 km^2
Number of detectors	~ 1600	~ 500
Lattice distance, structure	1.5 km, hexagonal	1.2 km, square
Detector Type	water Cherenkov	Plastic Scintillator
Detector Size	10 m^2 $\times$ 1.2 m	(2$\times$) 3 m^2 $\times$ 1.2 cm
Detector sampling	25 ns	20 ns
Fluorescence Detectors		
Number of sites	4	3
Number of Telescopes	24	36
Size of each Telescope	13 m^2	6.8 m^2/3 m^2
Field of view	28.5° $\times$ 30°	16° $\times$ 14° /18° $\times$ 15°
Number of pixels	440	256

http://www.telescopearray.org/

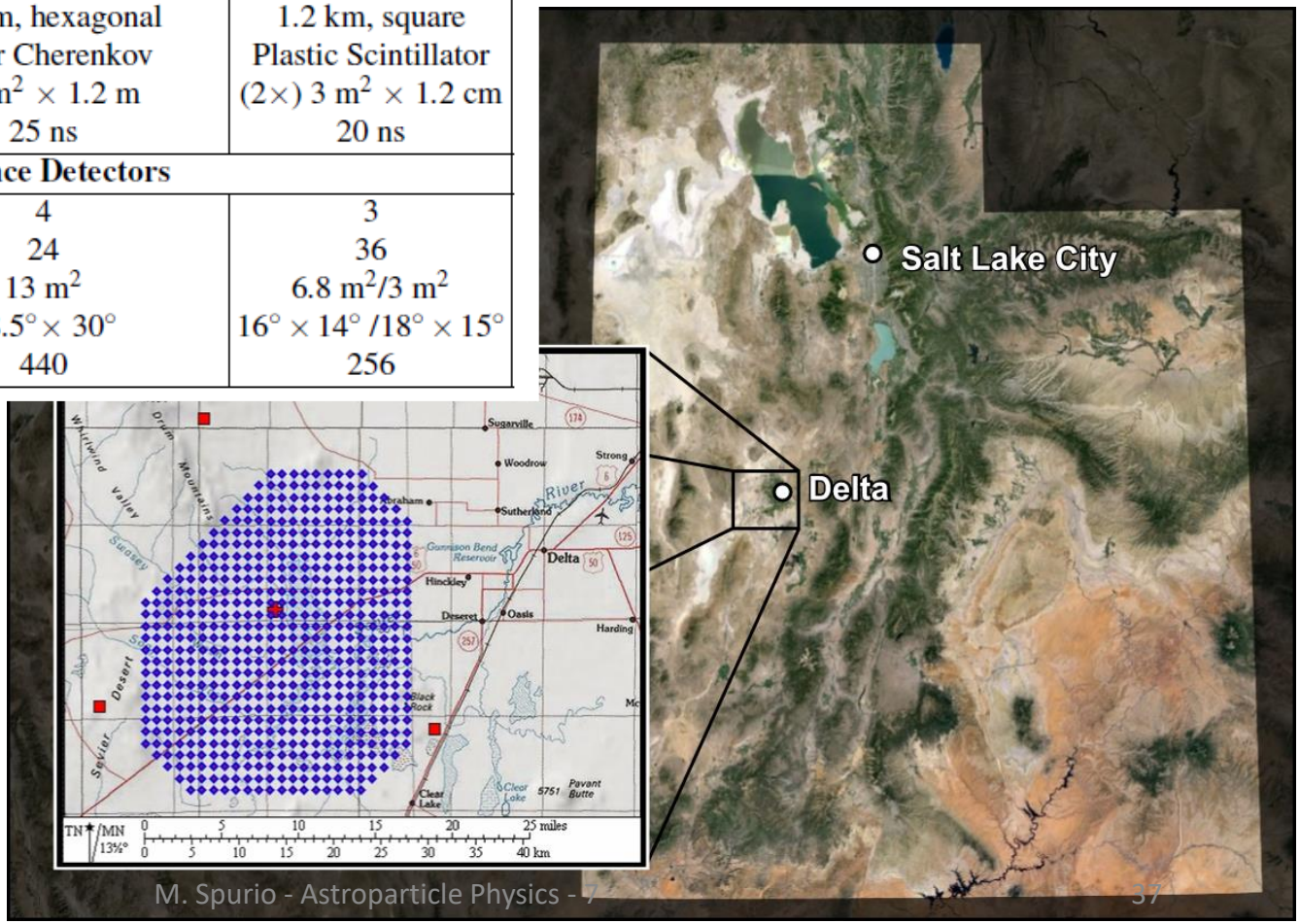

UHECRs spectrum from AUGER

Number of events. Notice the discontinuity (low energy events measured with a low-energy extension of PAO)

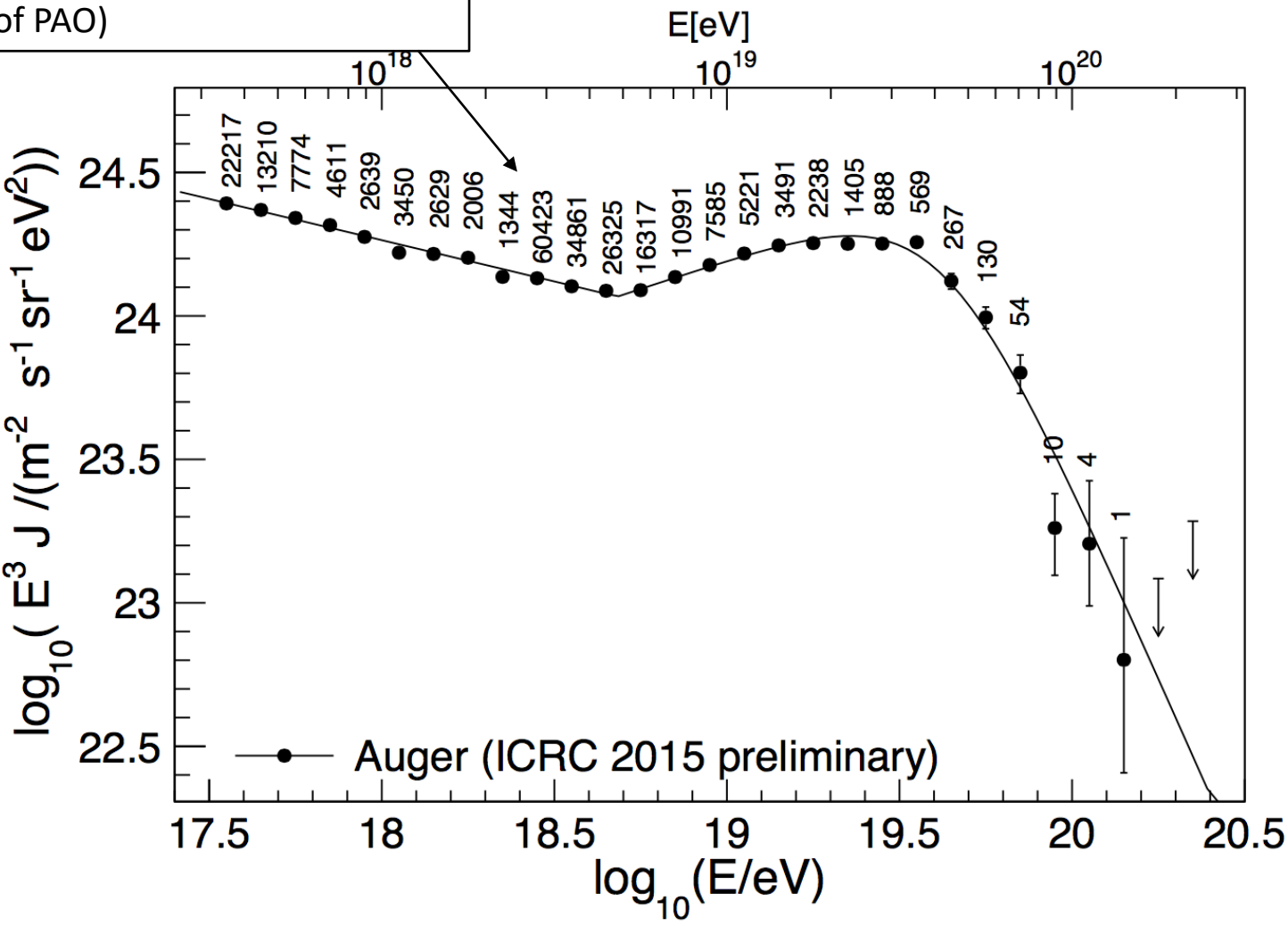

Summary of the results (and a warning!)

- **Beware of the plots.** It is common to present the CR flux (power law) multiplied by E^k .
- In this representation, features such as the ankle at $10^{18.5}$ eV are more evident.
- However, it should be emphasized that **scaling** the flux with **energy to some power could induce a bias** regarding the interpretation of the results from the visual inspection of the figure. Let consider the **case k=3,** as in this figure.

- Each experiment quote a systematic uncertainty ΔE on the estimated energy E.
- Points referring to this experiment can be shifted along the x-axis by $\pm\Delta E$.
- Consequently, points along the y-axis must also be shifted by a quantity $(1 \pm \Delta E/E)^3$.
- As an example, if the AGASA points suffer from a 25% systematic overestimation of the energy, all points should be shifted left by a factor of 0.75 E along x and pushed down by $(0.75)^3$ = 42% along y.
- The arrow in Fig. indicates such a 25% shift

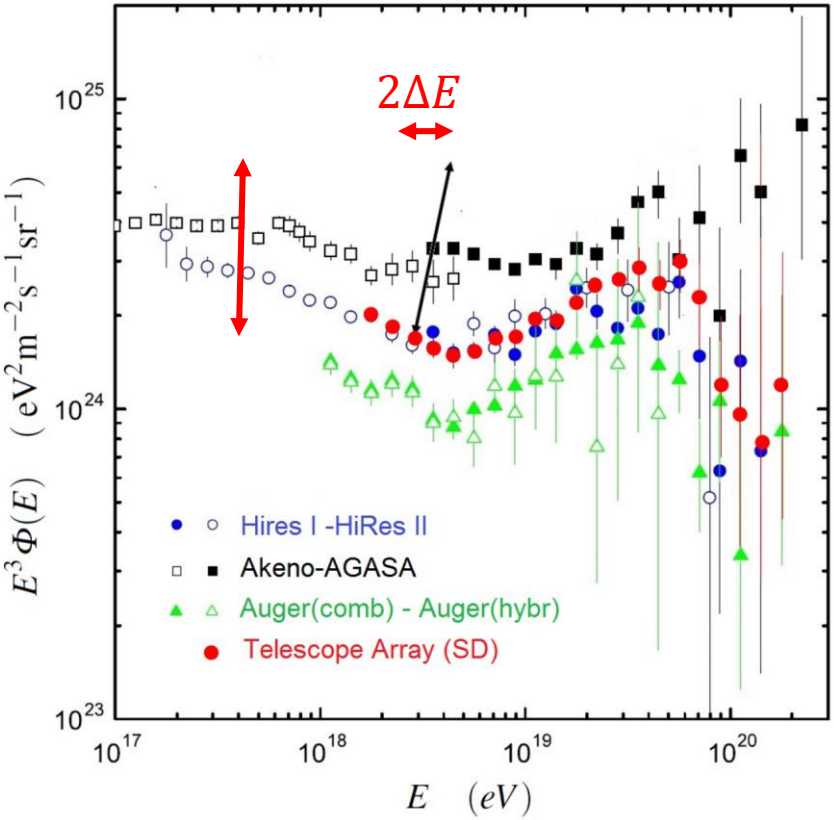

Data and Possible source models (one example!)

- The same data, after rescaling the energy of the experiments to obtain a common position of the "dip" at 5×10^{18} eV.
- The nominal energy scales multiplied by 1.2 (Auger), 1.0 (HiRes), 0.75 (AGASA), 0.95 (TA) and 0.625 (Yakutsk)

Predictions

- Red: "dip model", due to extragalactic p.
- **Blue line**: "superposition model" with a galactic (dashed) + extra-galactic component (full line)
- The softening of the spectrum at E> 5×10^{19} eV observed by HiRes, PAO and TA is consistent with the GZK effect,
- BUT, It **does not** necessarily represent a proof that the cut-off has been discovered. The GZK cut-off at ~10^{20} eV implies that UHECRs are protons, and not heavier nuclei

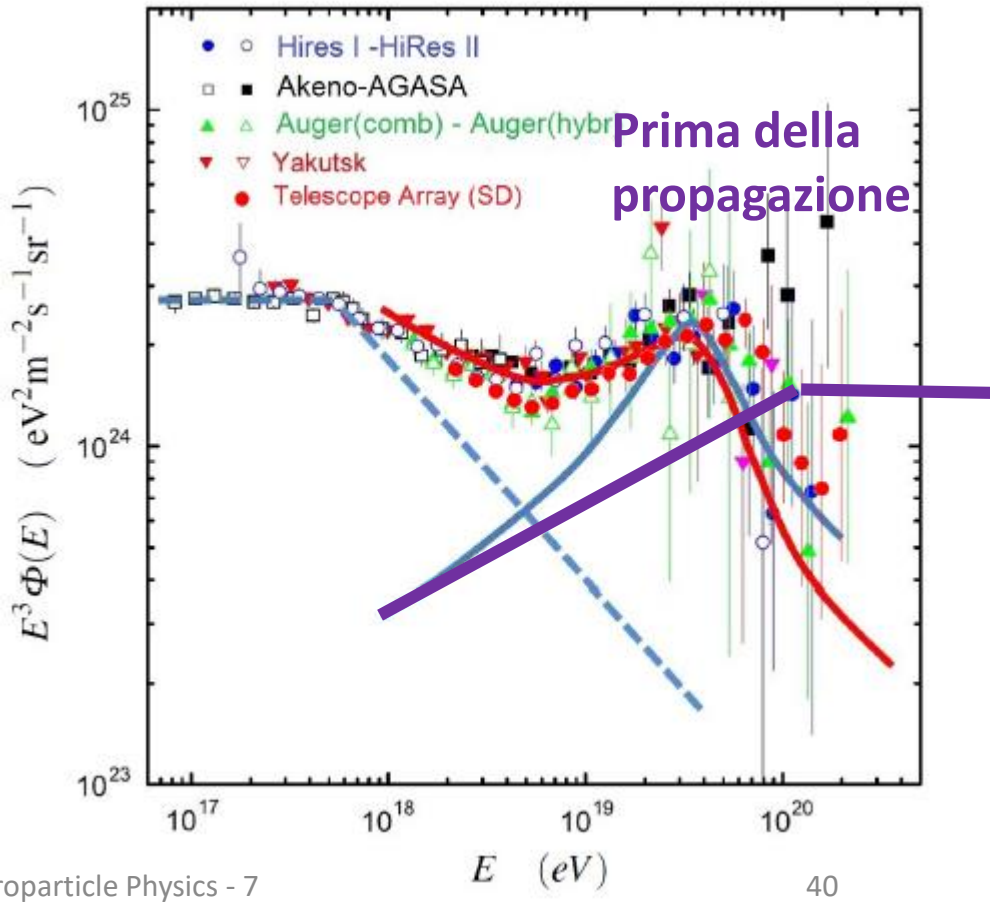

The Chemical Composition of UHECRs

- The determination of charge (or mass) of the incoming primary UHECRs is difficult.
- Shower-to-shower fluctuations prevent the individual measurement of mass number, A.
- The general features of a heavy nuclei cascade are (Sect. 4.4.4):
  - (i) the showers reach their maximum development, X_{max}, higher in atmosphere,
  - (ii) they generate more muons than showers induced by a proton primary of equivalent energy.
- The discrimination between the arrival of a proton or that of a heavier nucleus relies thus on the observation of either the **longitudinal development** of a shower or by the simultaneous determination of the **EM and muonic** components of EAS at ground level.
- Unfortunately, the former technique can be used only on clear, moonless nights and suffers from the lack of statistics at the highest energies.
- The first analysis of the X_{max} vs. energy with fluorescence detector data was done with the Fly's Eye, then by HiRes and followed by PAO and TA

CORS

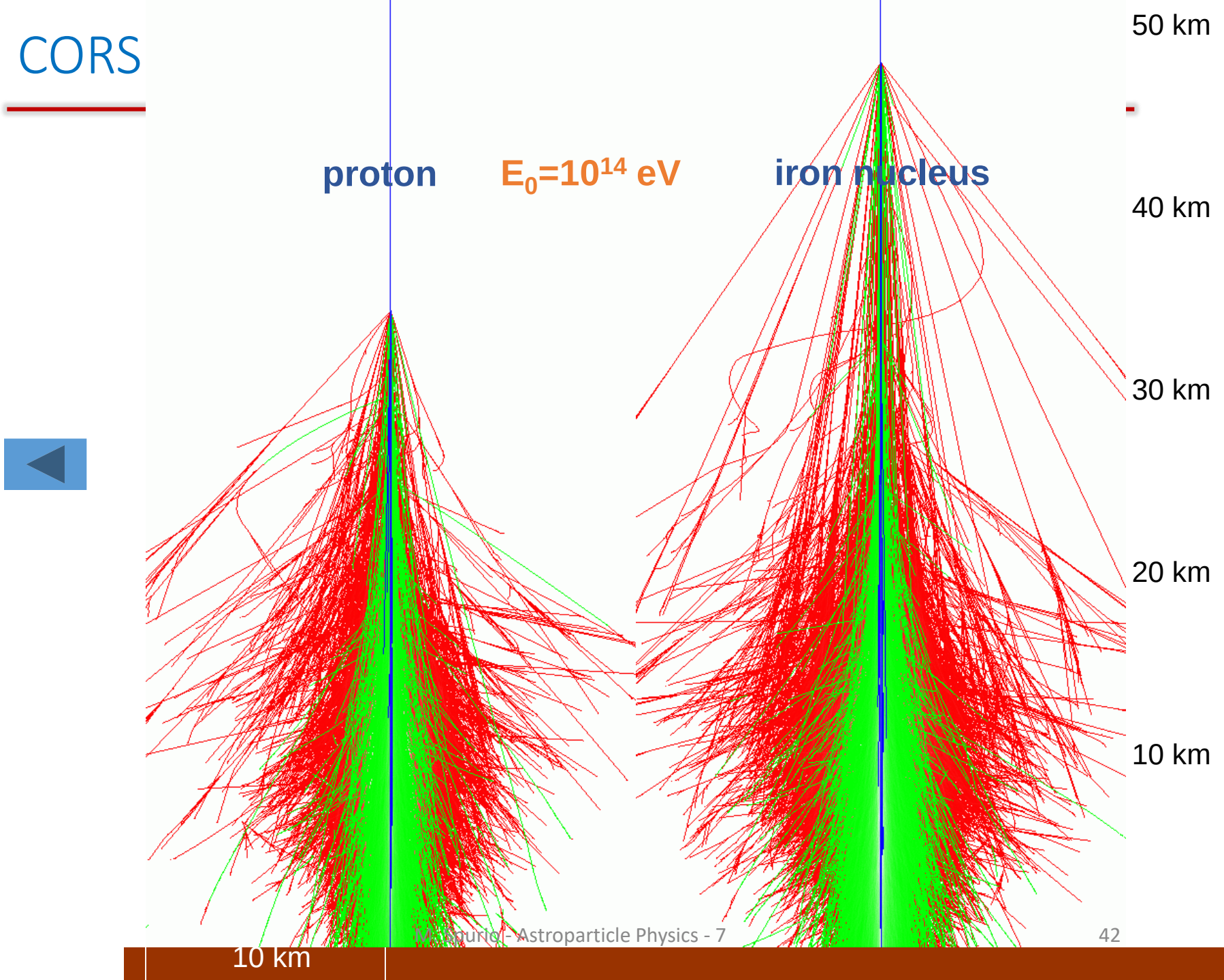
proton
$E_0=10^{14}$ eV
iron nucleus
50 km
40 km
30 km
20 km
10 km
e/γ
μ
h
10 km

The X_{max} measurement for UHECRs (2018)

- The HiRes result suggested a quick transition from heavy to light cosmic ray composition above a few 10^{18} eV.
- The Telescope Array measurement (not shown) is consistent with that of HiRes.
- The PAO results are somewhat in disagreement with those of HiRes and TA. In their data, the CR composition becomes lighter up to $2x10^{18}$ eV and then consistently heavier up to the highest energy measured.

- Note that the data in Fig. terminate before the energy of GZK effect.
- The chemical composition of CR above $5x10^{19}$ eV is unknown, although PAO suggests a significant fraction of heavy nuclei.
- Work for future generations of physicists

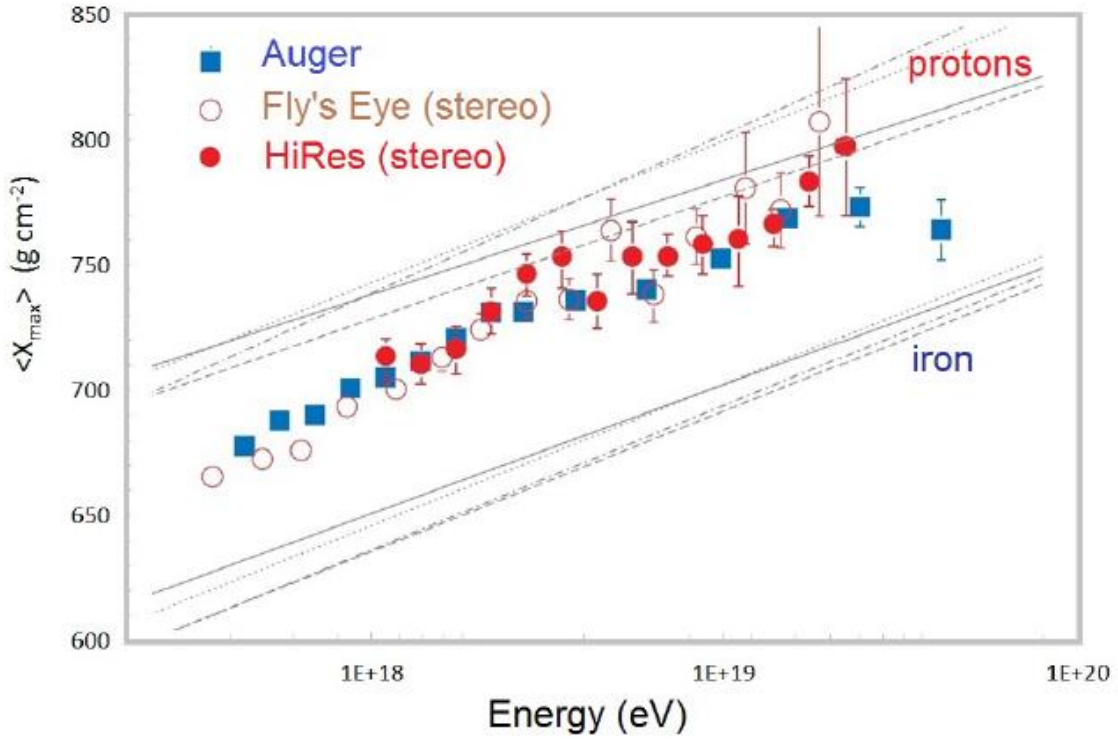

Mass Composition of CRs Around the Knee (Chap. 4)

- As discussed, it is particularly difficult to determine the mass number, A
- At least two independent quantities have to be measured to estimate **energy** and **mass** of the primary CR that initiated the EAS.
- In addition to the shower size Ne, the position X_{max} of the maximum or the muon size Nμ are usually observed.

- The measurement is difficult on a shower-to-shower basis, due to the intrinsic fluctuation (at a fixed Ne) of X_{max} and Nμ.
- Unfolding methods are usually employed

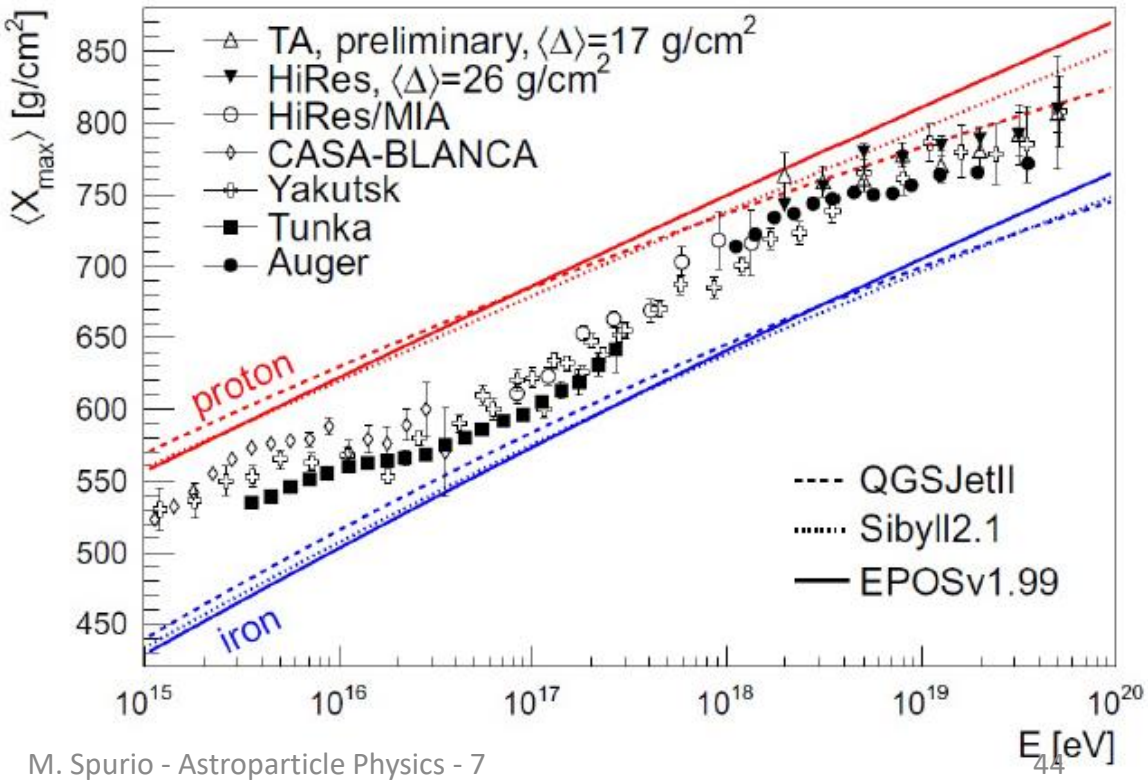

Sources?

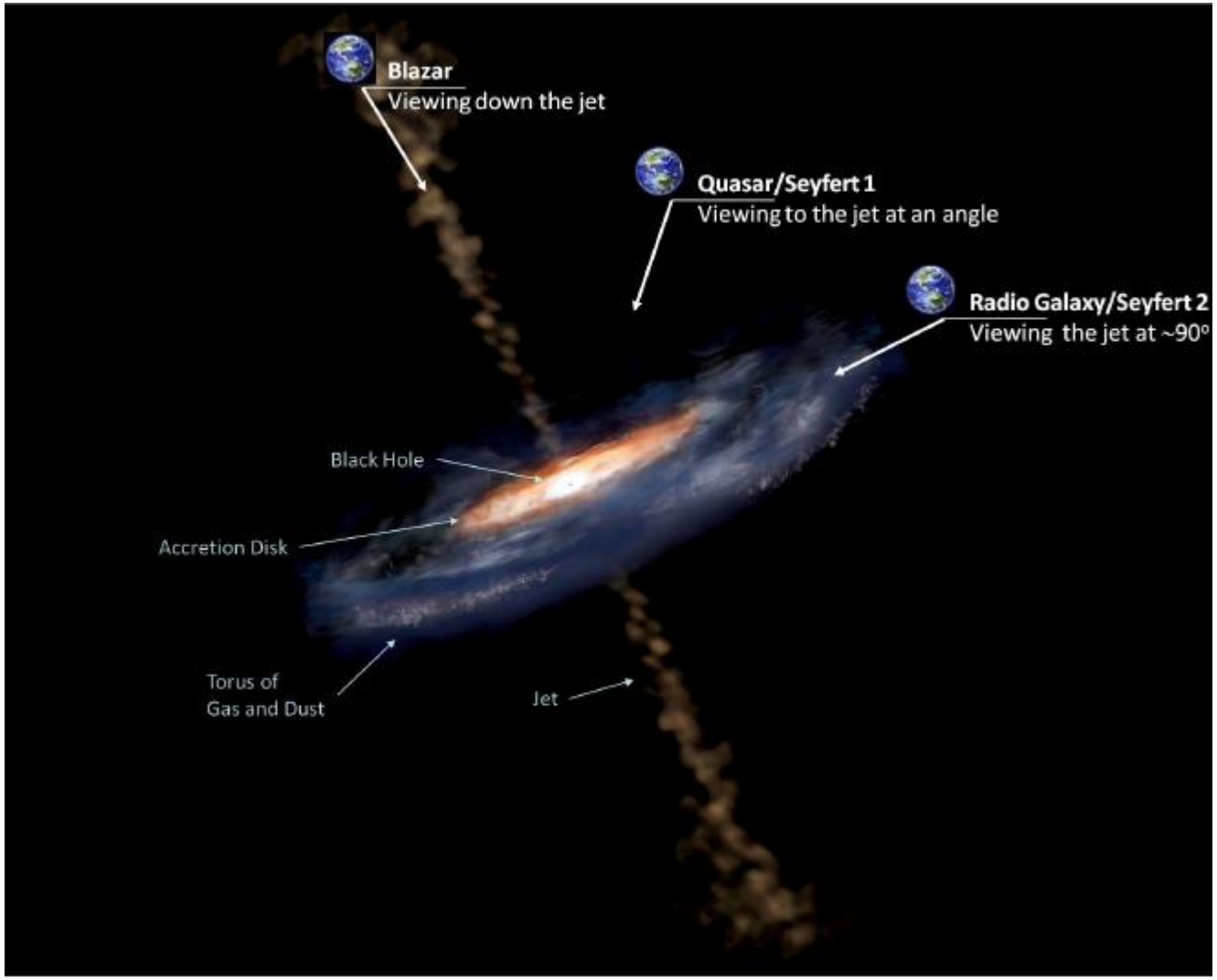
Blazar
Viewing down the jet
Quasar/Seyfert 1
Viewing to the jet at an angle
Radio Galaxy/Seyfert 2
Viewing the jet at ~90°
Black Hole
Accretion Disk
Torus of
Gas and Dust
Jet